

FUNDAMENTAL FORCES IMPORTANT TO  
THE ENHANCEMENT OF BIOLOGICAL COLLOID REMOVAL

By

STEPHEN E. TRUESDAIL

A DISSERTATION PRESENTED TO THE GRADUATE SCHOOL  
OF THE UNIVERSITY OF FLORIDA IN PARTIAL FULFILLMENT  
OF THE REQUIREMENTS FOR THE DEGREE OF  
DOCTOR OF PHILOSOPHY

UNIVERSITY OF FLORIDA

1999

To my father and the three ladies of my life,  
my wife, my mother, and my grandmother.

## ACKNOWLEDGMENTS

I would like to express my deep gratitude to the many individuals with whom I have had the opportunity to work during the course of my doctoral studies. I thank Dr. Richard Dickinson for his selfless efforts in mentoring my research and Dr. Dinesh Shah for his contribution to my communication and networking skills. A special thanks has been reserved for Dr. Gerald Westermann-Clark and Dr. Vinod Pilli for their intellectual camaraderie and friendship. Their passing marks a significant loss to the scientific community.

In addition, I would also like to thank Dr. Brij Moudgil and the members of the Engineering Research Center, Advance Separation Processes group; specifically Dr. Hassan El-Shall and Dr. James Adair for their support and friendship, Dr. Samuel Farrah and Dr. George Lukasik for their assistance within the microbiological field, Dr. Yongchen Li for his participation in many scientific discussions, Josh Adler for his tireless pursuit of science and Alex Patist for being European, but mixing like a Russian.

I would like to acknowledge the financial support of the Engineering Research Center (ERC) for Particle Science and Technology at the University of Florida, National Science Foundation (NSF) grant #EEC-94-02989.

## TABLE OF CONTENTS

ACKNOWLEDGMENTS.....	iii
LIST OF TABLES.....	vii
LIST OF FIGURES.....	viii
ABSTRACT.....	xi
CHAPTERS	
1 BACKGROUND.....	1
1-1 General Introduction.....	1
1-2 Introduction to Interparticle Forces Through the Context of DLVO Theory ..	2
1-3 Critical Issues Inherent to DLVO Theory.....	5
1-3-1 The Double Layer Term of DLVO .....	5
1-3-2 The van der Waals Term of DLVO .....	7
1-3-3 Hydrophobic Interactions.....	8
1-3-4 Fimbriae and Pili Mediated Interactions.....	9
1-4 Dissertation Organization.....	10
2 MEASUREMENT OF PACKED BED ELECTROKINETICS.....	11
2-1 Introduction.....	11
2-2 Theoretical Background.....	11
2-3 Accuracy and Precision.....	15
2-4 Characterization of Metal Hydroxide Coatings.....	17
3 MICROORGANISM CHARACTERISTICS AND ELECTROKINETICS.....	26
3-1 General Background on Microorganisms.....	26
3-2 Bacterial Electrostatics.....	28
4 EVALUATION OF DLVO THEORY THROUGH SIMPLE BACTERIAL DEPOSITION STUDIES .....	34

4-1 Introduction.....	34
4-2 Preparation and Characterization of Surfaces.....	35
4-2-1 Granular Surface Preparation.....	35
4-2-2 Granular Surface Characterization.....	36
4-2-3 Bacterial Preparation.....	37
4-2-4 Bacterial Surface Potential.....	38
4-3 Deposition Measurements.....	38
4-4 DLVO Calculations.....	40
4-5 Results.....	43
4-5-1 Deposition Results.....	46
4-5-2 DLVO Predictions.....	47
4-6 Discussion.....	50
4-7 Conclusion.....	53
 5 DIRECT MEASUREMENT OF INTERPARTICLE FORCES ON BIOLOGICAL COLLOIDS.....	 55
5-1 Background on Surface Force Measurements.....	55
5-2 Quantitative Measurements of Interparticle Forces.....	56
5-2-1 Three Dimensional Optical Trapping Evanescent Wave Light Scattering.....	57
5-2-2 Characterization of Interacting 3DOT-EWLS Surfaces.....	59
5-3 Bacteria/Glass Interaction Forces.....	59
5-4 DLVO Theoretical Predictions.....	62
5-5 Comparison of DLVO Theory to 3DOT-EWLS Experimental Data.....	62
5-6 Discussion.....	65
5-6-1 Failure of DLVO Theory to Match 3DOT-EWLS Bacterial Data.....	65
5-6-2 Compression of the Bacterial Cell Wall.....	69
5-6-3 Electrolyte Effects.....	71
5-7 Conclusions.....	71
 6 FEASIBILITY OF CHEMICAL MODIFICATIONS WITHIN 3DOT-EWLS STUDIES.....	 73
6-1 Introduction.....	73
6-2 Materials and Methods.....	74
6-2-1 Silane Surface Preparation.....	74
6-2-2 Surface Characterization.....	76
6-3 Results and Discussion.....	77
6-4 Conclusion.....	84
6-5 Summation.....	85
 7 CONCLUSIONS AND FUTURE WORK.....	 87
7-1 Colloidal Particles Under 3DOT-EWLS Analysis.....	87

7-2 Substrates Under 3DOT-EWLS Analysis.....	89
7-3 Investigation of Oil Emulsion Interactions with Solid Surfaces.....	90

#### APPENDICIES

A STREAMING POTENTIAL DESIGN AND OPPERATION.....	92
B ORIGIN OF CHARGE WITHIN THE METAL HYDROXIDES.....	98
C "OPTIMAL" PERFORMANCE.....	102

REFERENCES.....	101
-----------------	-----

BIOGRAPHICAL SKETCH.....	115
--------------------------	-----

## LIST OF TABLES

### Table

2-1	Validation of streaming potential device through the comparison of measured and reported values of zeta potential.....	17
4-1	Bacterial properties used in the calculation of DLVO energy curves.....	42
4-2	Values used in the calculation of the bacterial Hamaker constant.....	42
4-3	Granular collector surface properties and respective Hamaker values.....	42
5-1	Properties of interacting 3DOT-EWLS surfaces.....	62
5-2	Possible explanations accounting for observed deviations between experimental data and theory.....	67
6-1	Qualitative and quantitative observations made with 3DOT-EWLS for a silane modified and unmodified glass slide.....	83
C-1	Cost analysis of proposed metal (hydr)oxide coatings.....	104

## LIST OF FIGURES

### Figures

1-1	Hypothetical DLVO energy potential curves illustrating the energy barrier and transport limited particle interaction senerios.....	3
2-1	Diagram of the electrical double layer.....	12
2-2	Comparison of zeta values between an electrophoretic device and the in-house designed streaming potential apparatus on a granite sample.....	16
2-3	Streaming potential determined values of zeta potential for two commonly available granular media, Ottawa sand and Oglebay Norton sand.....	18
2-4	Proposed bonding mechanism of the precipitated metal hydroxide with the silica surface.....	19
2-5	Zeta potentials as measured by streaming potential device for the precipitate coated metal (hydr)oxide sands before long term water exposure.....	21
2-6	Zeta potentials for the various metal (hydr)oxide precipitate coatings after attritioning of coated samples on a spinning wheel for 30 minutes.....	21
2-7	Scanning Electron Microscope Elemental Microprobe Scan for aluminum on the mixed (hydr)oxide coating.....	22
2-8	Scanning Electron Microscope Elemental Microprobe Scan for iron on the mixed (hydr)oxide coating.....	22
2-9	Zeta potential as a function of exposure to chlorinated wastewater for the aluminum (hydr)oxide coated granular media.....	23
2-10	Zeta potentials as a function of pH for the aluminum (hydr)oxide coated Ottawa sand after multiple days of exposure to non-chlorinated wastewater. Biogrowth present.....	24



3-1	Bacterial cell membranes for Gram negative (Diagram A) and Gram positive (Diagram B) bacteria.....	27
3-2	SEM micrographs of the four microorganisms used within this study.....	29
3-3	Microbial zeta potentials as determined by electrophoresis.....	31
3-4	<i>Staphylococcus aureus</i> zeta potentials determined by electrophoresis as a function of aqueous solution ionic strength.....	32
4-1	Set of solubility curves for both the aluminum and iron species in water.....	36
4-2	Sample set of data representing the number of <i>E. coli</i> in the supernatant of the deposition studies as a function of time and exposure to various collector medias.....	40
4-3	Scanning Electron Microscope Elemental Microprobe Scan for iron on an unmodified Ottawa sand surface.....	45
4-4	Magnified Scanning Electron Microscope Elemental Microprobe Scan for iron on an unmodified Ottawa sand surface showing size of a patchwise impurity.....	45
4-5	Scanning Electron Microscope Elemental Microprobe Scan for aluminum on an aluminum (hydr)oxide modified surface.....	46
4-6	Comparison of the kinetic rate constants of deposition as determined with deposition studies.....	47
4-7	DLVO predicted energy curves for non-coated Ottawa sand and four microbes.....	49
4-8	DLVO predicted energy curves for iron (hydr)oxide coated Ottawa sand and four microbes.....	49
5-1	Diagram of the 3DOT-EWLS device.....	58
5-2	Three sample 3DOT-EWLS curves demonstrating the reproducibility of the bacterial force measurements for the <i>S. aureus</i> -glass system.....	61
5-3	3DOT-EWLS curves for <i>S. aureus</i> -glass slide system at three different electrolyte concentrations.....	61
5-4	Comparison of 3DOT-EWLS data with DLVO predictions.....	63

5-5	Comparison of experimental and theoretical interaction force decay lengths.....	64
5-6	Chemical composition of ribitol teichoic acid.....	66
5-7	Possible bacterial conformations within the 3DOT-EWLS optical trap.....	69
5-8	Diagram suggesting the reconfirmation of the bacterial membrane/bacterial polymeric projections upon experimental probing of a glass slide surface within the 3DOT-EWLS device.....	70
6-1	Deposition mechanism of silanes from aqueous media.....	75
6-2	Diagram of proposed final product of the three step silane reaction reported to have a pH independent surface charge.....	76
6-3	Graph showing streaming potential results for three modified surfaces as a function of water elution volume.....	78
6-4	Zeta potential as a function of pH comparing acid washed glass beads before and after coating with tetramethylcyclotetrasiloxane.....	79
6-5	Structure of TMCTS as compared to triethoxysilane.....	79
6-6	Comparison of zeta potential of N, N-dimethylbutylamine coating as a function of elution volume and initial silanization step used.....	80
6-7	Schematic representation of a possible multistep silanization reaction.....	80
6-8	AFM tapping mode results showing surface morphology of an unmodified glass slide and a 3-Aminopropyltriethoxysilane coated glass slide.....	81
6-9	3DOT-EWLS force and energy curves for colloidal silica and a 3-APTES modified glass slide at pH 6.3.....	83
6-10	Comparison of 3DOT-EWLS data for unmodified and a 3-APTES (after washing) coated glass surface interacting with colloidal silica for 0.1 mM KCl.....	85
7-1	3DOT-EWLS data for an emulsion droplet (SDS, hexadecane and water)...	91
A-1	Diagram A shows the streaming potential setup. Diagram B shows the electrode supports of the device.....	93

A-2	Sample data from the streaming potential device demonstrating the linear regression and 95% confidence interval used in the data analysis.....	96
-----	--	----

Abstract of Dissertation Presented to the Graduate School  
of the University of Florida in Partial Fulfillment of the  
Requirements for the Degree of Doctor of Philosophy

FUNDAMENTAL FORCES IMPORTANT TO THE  
ENHANCEMENT OF BIOLOGICAL COLLOID REMOVAL

By

Stephen E. Truesdail

May 1999

Chairman: Dr. Dinesh O. Shah

Major Department: Chemical Engineering Department

Microbiological colloids have very complex surfaces consisting of many proteins, varying degrees of surface roughness and in some cases even flagella and fimbriae appendages. These complexities have historically played a large role in preventing a thorough understanding of biological adhesion to surfaces. The DLVO forces (van der Waals and double layer forces), used to successfully describe many ideal non-biological colloidal interactions, are generally believed to be inadequate in describing microbiological colloidal forces. The importance of additional forces such as hydrophobicity, macromolecular receptor-ligand type binding and macromolecular forces arising from the presence of appendages or the polymeric bacterial surface have been suggested but not conclusively isolated as factors influencing bacterial deposition.

Traditionally, research within the area of particle adhesion has focused upon relating surface properties to experimental deposition trends. Many such studies have utilized pack bed filtration and parallel plate flow techniques in an attempt to quantify forces and identify surface properties important to microbial adhesion. Unfortunately, issues of statistical reproducibility have often times limited the usefulness of these types of approaches and their conclusions. The relative ineffectiveness of these deposition type experiments has served to highlight the need for a better approach in studying the complex interactions of microbiological particles. A new technique, Three Dimensional Optical Trapping Evanescent Wave Light Scattering (3DOT-EWLS), was developed and applied to directly measure these bacterial adhesion forces as a function of separation distance. The technique was used to measure the forces between a *Staphylococcus aureus* microbe and a glass microscope slide as a function of electrolyte concentration. Comparison between these measured interaction forces curves and the theoretically predicted force curves as based on DLVO theory showed significant disagreement. The theoretical curves appeared to overestimate the repulsive nature of the bacterial/surface interaction and suggested the importance of the bacterial surface projections in influencing particle Debye lengths important to bacterial adhesion to surfaces.

## CHAPTER 1 BACKGROUND

### 1-1 General Introduction

Microbial adhesion can be linked to numerous biomedical, commercial and industrial problems through product contamination, inefficient heat transfer, corrosion, infections and disease [Lit97]. Outbreaks of waterborn illnesses due to *Cryptosporidium* and *Giardia* microbes have also been linked to over 14,000 illnesses within the United States between the years of 1986 and 1988. A number which has remained strong well into the 1990's in spite of recent advances in commercial filtration systems [Smi93]. Bacteria are complex colloidal particles with a wide variety of properties often experimentally difficult to measure and model. Understanding the forces involved in microbial adhesion, can lead to specifically engineered surfaces with the ability to either promote or prevent adhesion in applications as diverse as water filtration, medical implant infections or corrosion. Bacterial adhesion, however, has been historically difficult to study at a fundamental level. This fact is at least partially attributed to the macroscopic nature of the many studies used to probe the microscopic forces important to microbial adhesion. Presently, hydration forces [Isr92], hydrophobic interactions [Ste89, vanL87a, vanL87b, Ger81], macromolecular receptor-ligand type binding [Dic97], surface roughness [Eli90, Sur97], surface appendages [Jon83, Ros82, Bas88], double layer and van der Waals forces [Kin93a, Kin93b, vanL90, Ver48] have all been proposed as possible contributors to the adhesion process. Of these various interaction forces, only

the double layer and van der Waals forces have a strong theoretical foundation in what has become known as DLVO theory by Derjaguin and Landau and independently by Verwey and Overbeek [Der41, Ver48].

### 1-2 Introduction to Interparticle Forces Through the Context of DLVO Theory

DLVO theory accounts for the contributions of double layer interactions and van der Waals forces to predict the potential energy of interaction between a particle and a surface; as illustrated in Figure 1-1. In the case of typical filtration systems where both the collector and the microbial contaminant are negatively charged, a repulsive energy barrier develops between the interacting surfaces, which can prevent particle deposition. The dashed line of Figure 1-1 represents this type of interaction where a large energy barrier would prevent attachment. As the magnitude of the surface charges decrease, DLVO theory predicts the van der Waals force will begin to dominate at short separation distances. At finite energy barrier around 10 kT, the energy barrier no longer prohibits particle deposition (solid center line) [Li97, Spi73]. For systems of sufficiently low energy barriers and systems of opposite charges where no energy barrier exists, the rate of deposition is controlled by the rate of diffusion or convective transport to the surface [Pri76].

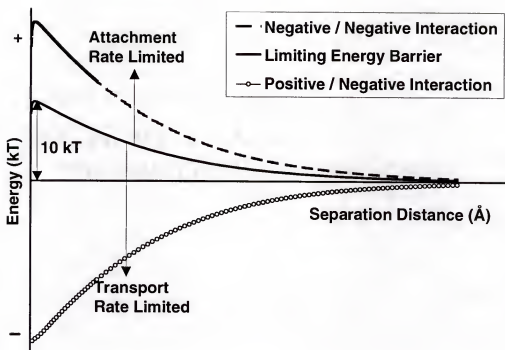


Figure 1-1. Hypothetical DLVO energy potential curves for oppositely charged particles (lower line) and similarly charged particles with increasingly larger charge magnitudes (upper dashed line). The solid center line represents the boundary between attachment rate limited deposition and transport limited particle deposition.

DLVO theory provides a convenient context to describe and predict particle deposition. Within this framework, double layer repulsion is responsible for preventing particle deposition. Many attempts to suppress or remove this repulsive force have been made to increase particle deposition and particle removal from aqueous streams [Mur80, Ste94]. Utilization of positively charged collector surfaces or the modification of existing collector surface with positively charged coatings should result in the removal of the energy barrier between the approaching microbe and collector surfaces. Apriori predictions of collector efficiency depend on the determination of particle and collector



surface potentials, a topic discussed in detail within Chapters 2 and 3. Overall cost, however, has historically prevented these types of modifications from reaching commercial and industrial application, a consideration also addressed within Appendix C.

The second approach to engineering systems capable of enhanced particle removal centers around the assumption that DLVO theory adequately describes all of the forces important to bacterial deposition, as biological particle interactions can be extremely complex. The double layer and van der Waals forces may not be the only important forces involved. However, attempts to correlate microbial surface properties and deposition behavior in terms of DLVO theory have had limited success. This has primarily been due to the fact that the batch deposition and column flow through experiments designed to study these microscopic biological interactions have only been able to provide “macroscopic” information, i.e., the measurements reflect average properties of the bacteria and collector surfaces. The insensitivity of these deposition experiments under even well defined conditions as suggested in Chapter 4 emphasizes the need to describe the interactions between biological colloids and solid substrates through the direct measurement of forces (Chapter 5). A new surface force technique termed Three Dimensional Optical Trap Evanescent Wave Light Scattering (3DOT-EWLS) was developed for this purpose [Cla99]. The experimental measurement of interparticle forces as a function of separation distance allows direct comparison between experimentally measured particle interactions and DLVO predictions. These comparisons are the first of their kind for microorganisms and are used to judge the accuracy of DLVO theory in describing microbial adhesion.

### 1-3 Critical Issues Inherent to DLVO Theory

On a qualitative macroscopic scale many authors have noted that DLVO theory adequately accounts for the differences between transport-limited and energy-barrier limited systems [Mur80]. Additional authors have reported the importance of these energy barriers in controlling microbial adhesion [Abb83, Juc96, Sim88, Sch94]. In spite of this limited success, the theory's ability to quantitatively describe bacterial surface forces has been called into question [Hul69, Isr92, Eli95]. DLVO theory does, however, serve as a reasonable starting point for studies on microbial deposition, although it relies on several assumptions and simplifications detailed below.

#### 1-3-1 The Double Layer Term of DLVO

The repulsive double layer portion of the DLVO theory is based upon the solution of the nonlinear Poisson-Boltzmann (PB) equation,

$$\frac{d^2\phi}{dx^2} = -\left(\frac{e}{\epsilon}\right) \sum z_i \eta_{i\infty} \exp\left(\frac{-z_i e \psi}{kT}\right) \quad (1.1)$$

where  $\phi$  is the interaction potential,  $x$  represents distance,  $e$  is the charge of an electron,  $\epsilon$  is the permittivity of the solution,  $z_i$  is the valence of the ionic species present,  $\eta_{i\infty}$  is the bulk number density of ions in solution,  $\psi$  is the surface potential,  $k$  is Boltzmann's constant and  $T$  is temperature. Some of the assumptions surrounding the solution of this equation may affect comparisons between theory and the observed microbial interaction. Solutions based upon the linearization of the PB equation above are applicable only for simple geometries such as spheres and flat plates. Solutions of the equation for irregularly shaped interaction species are much more difficult although several other

geometrical solutions have been reported in the literature such as for cylindrical geometries [vanK95, Kuy98] which could be used to represent rod-shaped microbes. Another assumption generally made with regards to the PB equation limits its use to solutions with 1:1 electrolytes. Several authors have attempted to provide solutions to the PB equation for divalent electrolytes with various numerical approaches [Mar92, Gil95, Ran84, Ake90, Hsu94].

Additional concerns about the double layer part of DLVO theory center around the measurement of surface potential. The common practice of approximating surface potentials through the measurement of zeta potentials is not strictly valid in the presence of even minute amounts of electrolyte. Realistically, the zeta potential should be viewed as a lower limit of the surface potential and may in fact result in an under representation of the repulsive force (Section 2-2). In addition, the under representation of the surface potential also arises from a phenomena commonly referred to as surface conduction or double layer polarization. Although this effect is present in all electrokinetic measurement techniques used to determine zeta potential, it is most commonly addressed in electrophoresis measurements [Ego94, van96]. Additional authors have also pointed out that this polarization of ions within the electrical double layer may also occur within the semi-porous microbial cell wall/membrane (Section 3-2). Charge migration due to the lateral mobility of proteins within the bacterial wall is also unaccounted for in the measurement of surface charge, although it has been reported by several authors [Jac75, Tat87, Ait81, Mur97, Hon84].

Solution of the PB equation also assumes uniform charge density of the surfaces involved and ignores the concept of charge smearing due to charge heterogeneity. A few

researchers have studied the importance of charge heterogeneity within the bacterial surface [Sim88]. Much more work, however, has been done on analyzing the possible importance of charge heterogeneity on solid substrates and its role in particle adhesion [Bow79, Eli90, Lit92].

### 1-3-2 The van der Waals Term of DLVO

The van der Waals interaction consists of three components, the London (dispersion) term, the Keesom term and the Debye term. Lifshitz theories (retarded and non-retarded) are used to determine the van der Waals interaction potential used in the DLVO expression. Lifshitz theory is based on continuum mechanics and treats the surface and the intervening solvent medium as a structureless continuum which does not account for molecular effects such as solvation forces or surface structure effects. Steric hydration forces and hydrophobic interactions are thought to dominate over double layer and van der Waals forces at small separations distances in biological systems [Isr92] and are unaccounted for within the DLVO expression [Ran84, Pop89]. Other research has centered around the errors associated with using a constant dielectric constant as opposed to one dependent on particle separation distance and corresponding solvation forces. Disagreements between values used to represent the fixed bacterial dielectric constant are also a point of debate and values are typically estimated between two extremes: 80 representing water and 2 representing the dielectric of protein [Isr92, War94, Sim91a, Sim91b, Lof97]. (Direct dielectric measurements through impedance analysis as a function of frequency from ~100 HZ to ~1 Hz are not possible without destruction of microbial membranes.)

The refractive index required to calculate the van der Waals force, is often estimated to reflect the proteins within the microbial cell wall and cell membrane (1.5 - 1.6) [Isr92]. The van der Waals force is relatively sensitive to changes within this parameter and as to date very little work has been done to determine bacterial refractive indices [Dyo96, Jon97, Tum97]. It is unclear, for example, whether the refractive index of the proteins within the membrane surface are solely responsible for the van der Waals interaction or if water and other cell structures combine with the membrane proteins to produce an average refractive value for the microbe as a whole.

The use of non-retarded Lifshitz theory also results in some uncertainty within the DLVO prediction of interaction forces [Hie97]. This is due to an inaccurate representation of the London (dispersion) component of the van der Waals force. The less complex non-retarded Lifshitz theory has a  $1/r^6$  dependence on separation distance as opposed to the more accurate representation of this force as a function of  $1/r^7$  [Isr92]. This retardation effect of the London component is quite large in the case of hydrocarbons and presumably therefore for biological surfaces. As a result the Hamaker constant is not really a constant but actually decreases with increasing separation distance.

### 1-3-3 Hydrophobic Interactions

Hydrophobic interactions are somewhat more controversial in their importance with regards to general interparticle forces. The fact that the DLVO theory fails to address hydrophobic forces has led to an alternative method of analyzing particle interactions often referred to as the Gibbs free energy balance [Mur80, Ben80, vanL90, Kre89]. The lipopolysaccharide layers of the bacterial cell wall and outer membrane

consist of proteins which have varying degrees of non-polar character. The resulting free energy (or entropic) driving forces from the solvation of these structures by aqueous media may play a part in overall particle interactions [Ste89, vanL87a, Van90, Ash86, Ron90]. The hydrophobic force has even been reported to be on the order of 10 to 100 time larger than the van der Waals force under certain idealized conditions [Pas85].

#### 1-3-4 Fimbriae and Pili Mediated Interactions

Surface appendages extending from the bacterial membranes also have been reported to play a role in microbial interactions [Juc98]. Fimbriae and/or flagella may promote attachment by spanning the repulsive energy barriers between two negatively charged surfaces. It has been theorized that these bacterial appendages can more easily approach a surface due to their small surface areas (correspondingly lower repulsive energy barriers) and/or through the attractive hydrophobic nature of these appendages [Bri65, Rob77]. Analysis of isolated fimbriae of certain bacterial species (Neisseria, Moraxella and Pseudomonas) show very strong hydrophobic character [Pea80]. Other authors have reported a direct correlation between adhesion, fimbriae/pili and hydrophobicity [Gal87, Bal88, Gil91, Ste89, She85, Nai93, Ste85, Wat92, Dru89, Don91, Nas97]. In short, these appendages create a much more complex interaction systems which may serve to either promote (polymer mediated bridging or flocculation) or prevent (steric repulsion) particle deposition.

#### 1-4 Dissertation Organization

Because of the complexities outlined above, microbial deposition is difficult to understand from a theoretical perspective. The majority of the literature does however, concede the importance of both van der Waals and double layer forces in particle interactions. DLVO theory is therefore often used as a convenient conceptual construct for fundamental work in the area. A major goal of this current research has been to evaluate the usefulness of DLVO theory in describing microbial adhesion to solid surfaces. In doing so, the first several chapters of this document have been devoted to the analysis of the surface properties important to DLVO theory (Chapters 2-3). This characterization has then been followed by a study attempting to quantitatively analyze bacterial deposition to granular media, Chapter 4. The failure of this type of deposition study to quantitatively identify the relative importance of forces involved in bacterial adhesion emphasizes the need for a direct force measurement between microorganisms and the solid substrate. Chapter 5 addresses the application of a technique (Three Dimensional Optical Trapping Evanescent Wave Light Scattering, 3DOT-EWLS) to provide the first direct force measurements between a single bacterium and a flat surface as a function of separation distance. The applicability of the DLVO theory to describe this interaction between a microbe and a surface was subsequently evaluated as based upon the quantitative 3DOT-EWLS data. The study of bacterial interactions to silanated glass were then evaluated in Chapter 6 in the hopes of successfully controlling and manipulating surface properties of the EWLS glass to broaden the range of surface forces potentially studied by the 3DOT-EWLS technique. Chapter 7 then addresses other potential applications of the 3DOT-EWLS technique as future work.

## CHAPTER 2 MEASUREMENT OF PACKED BED ELECTROKINETICS

### 2-1 Introduction

Zeta potential/surface charge of granular media is another relevant parameter in particle deposition. The development and success of DLVO theory in describing dispersion stability has served to highlight the importance of zeta potentials in particle interactions [Der41, Ver48]. The measurement of zeta potential, although well developed theoretically [Ove52, van80], has historically been problematic. A few relatively complex streaming potential devices have been developed within the past several years in an attempt to reduce analysis time and enhance data acquisition [Fit72, Fai91, Sca92]. For systems of membranes, capillaries and flat plates, where sample equilibration time can be quite short, these systems appear to be fairly efficient. Granular systems, however, often suffer from complications requiring longer equilibration times. This chapter describes a procedure for building and operating a very simple streaming potential device to measure the zeta potential of granular media accurately and reproducibly. This specific apparatus design is intended for use with granular materials and has intentionally been developed in a simplistic manner to encourage wider usage.

### 2-2 Theoretical Background

Surface charge refers to the charge character of a surface due to its actual molecular composition. Zeta potential is a term used to describe the potential due to that



charge at some finite distance away from the surface at what is termed the plane of shear. At this plane the potential is somewhat smaller in magnitude than the surface potential due to ion association of the surrounding solution (the electrical double layer, Figure 2-1). Under idealized conditions of dilute electrolyte concentration, the number of these associating ions shielding the surface charge are very few and the zeta potential and surface potential are generally assumed to be identical.

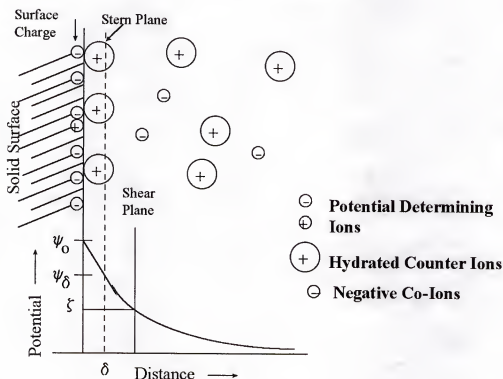


Figure 2-1. Electrical double layer [HIE97].

This allows for a relatively easy estimation of surface potential through the measurement of zeta potential with the streaming potential instrument. Unfortunately, much of the work presented in the literature tends to favor electrophoresis, an instrument used to measure electrophoretic mobility of very small particles from which zeta potential can be calculated. The act of grinding or crushing large particles for use in electrophoresis,

particularly those in which the surface composition differs from the inner bulk material as in the case of coatings and biogrowth, will lead to an incorrect evaluation of the larger particle's surface potential. It is for this reason that a particular emphasis should be placed on the proper design and usage of a streaming potential device for reproducible evaluation of the zeta potential on granular media.

The theory behind the streaming potential apparatus is rooted within irreversible thermodynamics. By allowing a charged solution to physically flow past a charged surface, a potential is created due to motion of the ions within the electrical double layer of the granular material. For systems near equilibrium the fluxes are expected to be linearly dependent on specific driving forces. Ohm's law, Darcy's law and Fourier's law are well-known examples of the linear relationship between conjugate forces and fluxes of a system. When these expressions are made to incorporate non-conjugate driving forces (i.e., forces usually assumed to be negligible), a set of equations is developed from which all electrokinetic phenomena can be described. In the case of the streaming potential, the incorporation of the non-conjugated terms within Ohm's law results in an expression that can be used to describe the system [van80],

$$\frac{I}{A} = L_{11} \frac{dE}{dx} + L_{12} \frac{d \ln C}{dx} + L_{13} \frac{dP}{dx} \quad (2.1)$$

where  $I$  = electrical current,  $A$  = area,  $L_{ik}$  = phenomenological coefficients,  $E$  = electromotive potential,  $C$  = concentration of the electrolyte,  $P$  = pressure and  $x$  = dependent length variable. The first phenomenological coefficient  $L_{11}$  can be represented as  $K$ , the specific resistivity of the electrolyte, through the realization that equation (2.1) must reduce to  $E=I/KA$ , electromotive potential equaling the product of current and resistance for a simple electrolyte system.  $L_{13}$  can then be shown to represent

the electrokinetic effect,  $\frac{\xi \epsilon \epsilon_0}{4\pi\mu}$ , through the use of Onsager's reciprocity relation ( $L_{ik} = L_{ki}$ ) and the linear expressions of the Darcy's law in terms of flux [Ove53] where  $\xi$  = zeta potential,  $\epsilon_o$  = viscosity of the electrolyte solution,  $\epsilon$  = dielectric constant of the electrolyte and  $\epsilon_o$  = dielectric constant of a vacuum. Further simplification of equation (2.1) can be made under the assumption that the concentration gradient of electrolytic species throughout the streaming potential's sample bed remains a constant during operation so that the  $\frac{d \ln C}{dx}$  term can be set to zero. Additional recognition that no electrical current is applied during the streaming potential operation ( $I = 0$ ) allows for final simplification. The resulting equation relates voltage drop across the material within the sample cell as a linear function of pressure drop in what is known as the Smoluchowski equation in cgs units [Hie97],

$$\xi = \frac{4\pi\mu K}{\epsilon\epsilon_o} \frac{\Delta E}{\Delta P} \quad (2.2)$$

where  $\Delta E$  represents the change in electromotive potential (voltage) and  $\Delta P$  is the corresponding change in pressure.

Application of streaming potential theory also requires the use of pressure drops within the regime of laminar flow in order to avoid random voltage instabilities created by turbulence and eddy formation within the packed bed's electrical double layer. This laminar restriction is widely found within the literature but has often been overlooked in application. The Reynold's equation [Bir60] can be used to calculate a conservative criterion of the superficial velocity ( $V_o$ ) for a granular system under laminar conditions:

$$Re = \frac{D_p V_o \rho}{(1-e)\mu} < 1 \quad (2.3)$$

where  $D_p$  = particle diameter,  $\rho$  = density of the liquid media (water) and  $e$  = void fraction of the packing. The limiting superficial velocity for the system under investigation is in turn applied as a restriction to the Burk-Plummer equation [Bir60],

$$\frac{\Delta P}{L} = \frac{150\mu V_o(1-e)^2}{D_p^2 e^3} \quad (2.4)$$

where  $L$  = length of the packed bed. This allows for an estimation of the upper pressure drop limit corresponding to the laminar flow regime, which should not be exceeded during streaming potential measurements. The onset of turbulent behavior will result in a disturbance of the electrical double layer of the of the sample and the possibility of unstable readings from the streaming potential apparatus. For the granular media used within this study (0.6 to 0.7 mm diameter) a maximum pressure drop of 7 cm of water was calculated as a conservative upper bound for the laminar flow.

### 2-3 Accuracy and Precision

In order to demonstrate the reliability of the measurement technique detailed in Appendix A, a comparative study was conducted on a granite sample. Half of this sample was crushed into micro particles and used in an independent measurement of the zeta potential [Els97]. Note that in this case the interior and exterior of the granite samples were expected to have the same composition. The other uncrushed portion of the granite sample (~0.7 mm diameter) was analyzed by streaming potential. The results are presented as Figure 2-2 over a range of pH. The comparison indicated a good match of the results obtained by the two techniques.

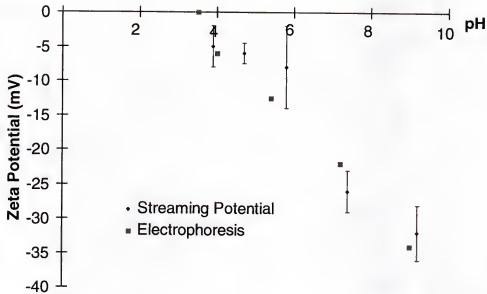


Figure 2-2 Comparison of two sets of zeta potential data as a function of pH for a granite system as determined by streaming potential and electrophoresis. The electrophoresis data (Brookhaven ZetaPlus instrument) were obtained from Global Consulting Company, Gainesville FL, unpublished data, no error bars provided.

Table 2-1 compares additional zeta potentials measured by this streaming potential apparatus with reported values for various materials and coatings. This apparatus provided reproducibility with an error generally on the order of  $\pm 10\%$  of the measured zeta potential using a 95% confidence interval as based on the pressure voltage slope determined for each run (Figure A-1) and a 95% confidence interval on the conductivity measurement of the electrolyte solution used in the measurement. The standard deviation among replicates was on the order of 3%. Exceptions did exist under conditions where the granular media was unstable. Passage of particle fines, coatings or microorganisms past the downstream electrode during measurement have the potential of significantly increasing the standard deviation of the measurement.

Table 2-1 Validation of streaming potential device through the comparison of measured and reported values of zeta potential

	pH	Experimental Zeta Potential	Referenced Zeta	Reference Source
Ottawa Sand (sieved & rinsed)	5.5	-68 ± 3mV	-65 mV	Electrophoresis
Pure Silica	5.6	-96 ± 3mV	-94 mV	[Goo90]
Silica modified with quaternary amine groups	6.65	45 ± 3mV	50 mV	[Suh95]
	5.3	47 ± 3mV	50 mV	
	4.3	44 ± 4mV	50 mV	
3-Aminopropyltriethoxysilane modified glass after water exposure	30L	15 ± 9mV	17 ± 3mV	Flat Plate Streaming Potential [Bat98]
	50L	0 ± 3mV	0 ± 3mV	
	90L	-7 ± 3mV	-9 ± 3mV	
Glass beads washed (Chromic acid/acetone/DI)	5.5	-140 ± 11mV	-136 mV	[Fit72]
Iron Hydroxide PZC (point of zero charge)		pH 7.5	pH 7.5	[Ada76]

Experimental zeta potentials were run on particles with roughly a 0.7 mm diameter (20-30 mesh).

#### 2-4 Characterization of Metal Hydroxide Coatings

The streaming potential technique has traditionally been used to estimate the surface potential of stable surfaces in which flow through the granular bed does not violate the assumption  $\frac{d \ln C}{dx} = 0$  of equation (2.1). Two such materials, Ottawa sand and Oglebay Norton sand have been evaluated and are shown in Figure 2-3 showing the pH dependent charge character of these two readily available granular materials. The observed differences in zeta potential between these sands served to highlight the importance of analysis on even compositionally similar materials. The negative Ottawa sand surface was chosen for further chemical modification and characterization.

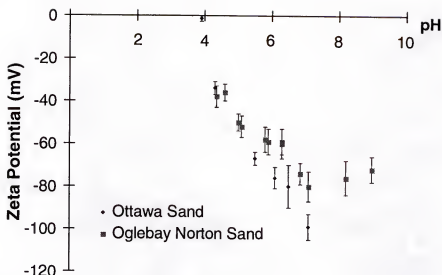


Figure 2-3 Zeta potential versus pH curves for Ottawa sand (Fisher) and Oglebay Norton sand (Brady, Texas). Both samples were 20-30 mesh in size.

Modifications to the Ottawa sand substrate were begun by soaking in 1M ferric chloride or 1M aluminum chloride solution for 30 minutes (all materials obtained from Fisher, Fairlawn NJ). The excess solution was drained and the sand was allowed to dry. The sand was then soaked in 2 volumes of 3 M ammonium hydroxide for 10 minutes, drained and allowed to air dry. The mixed coating was created through simultaneous treatment of the sand with the 0.25 M  $\text{FeCl}_3$  and 0.5 M  $\text{AlCl}_3$  and was subjected to similar washing and drying procedures [Luk97]. The following reactions were expected for these systems:



The actual crystal structures produced in these reactions were expected to contain the polymorphs of  $\text{FeO}(\text{OH})$  (which include Goethite, Akaganeite, Lepidocrocite, Ferrihydrite and Feroxyhyte) and  $\text{Al}(\text{OH})_3$  (which include Gibbsite, Doyleite, Nordstrandite and Bayerite) as well as some of the respective metal oxides (2.7-2.8) and hereafter have been denoted as (hydr)oxides. The surface precipitation reaction of the metal (hydr)oxides being suggested as:

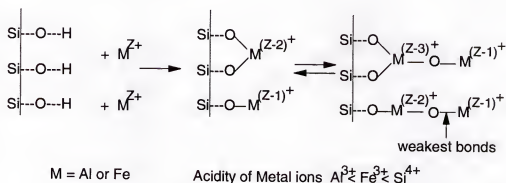


Figure 2-4 Bonding mechanisms of metal (hydr)oxides onto a silica surface. Anticipated deposition reactions are thought to greatly exceed the several monolayer shown here.

These precipitated metal (hydr)oxide coatings were expected to have positive surface potentials as predicted both theoretically [Hie96, Hie87] (see Appendix B) and experimentally [Par65].

Streaming potential was also used on these various metal (hydr)oxide coatings in order to approximate the surface charge for the theoretical development of the collector - microbe interaction systems. The following figure shows the zeta potential (approximation of surface potential) as a function of pH after washing the precipitated coated sample in a nylon mesh sieve tray under DI water (pH 6.3). Figure 2-5 shows an initial increase in positive charge character of the modified Ottawa sand surfaces. These



positive surfaces should lead to transport-limited deposition of negatively charged particles, with correspondingly high removal efficiencies. Simple end over end attritioning of these precipitated surfaces in water containing vessels on a 70 cm diameter vertical spinning wheel at 30 rev/min did show signs of coating loss from the surface after 30 minutes. The streaming potential results after attritioning are shown in Figure 2-6. Notice that upon comparison with Figure 2-5, the zeta curve for the mixed (hydr)oxide has shifted upward and now appears very similar to the aluminum (hydr)oxide coated surface. The iron (hydr)oxide curve has also shifted downward after attritioning. The streaming potential data indicated that the aluminum and the mixed surface coatings did retain a positive charge. The iron coating did not appear to be as strongly bound to the Ottawa sand surface under these precipitation conditions and shielded less of the negative surface charge of the underlying Ottawa sand substrate. This resulting negative - negative interaction of collector surface to bacteria is expected to result in some degree of energy barrier causing a less favorable interaction (solid line approaching the upper dashed line of Figure 1-1). The similarities in zeta potential between the mixed coating and the aluminum coating suggested the likewise loss of iron from the surface of the mixed coating. Follow-up scanning electron microscope elemental analysis confirmed this loss of iron. A comparison of elemental surface coverage of iron and aluminum for the mixed coating and the pure aluminum is shown in Figure 2-7 and 2-8. The weak iron signal also seemed to further support the theory that the iron was breaking free from the surface leaving an aluminum rich surface rather than the intended Al/Fe mix.

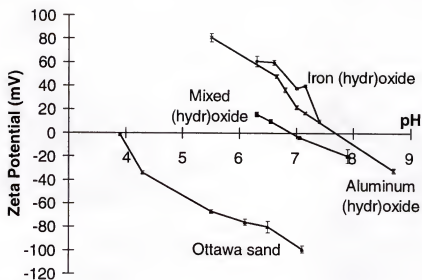


Figure 2-5 Initial results of zeta potential versus pH for (bottom to top) unmodified Ottawa, Mixed Aluminum/Iron (hydr)oxide coated, Aluminum (hydr)oxide coated and Iron (hydr)oxide coated Ottawa sands. Error associated with pH was determined to be  $\pm 0.15$  pH units.

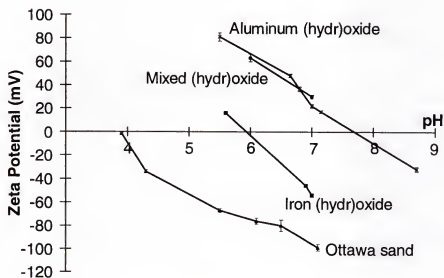


Figure 2-6 Zeta potential curves for various metal (hydr)oxide coated Ottawa sand surfaces after attritioning on a vertical spinning wheel for 30 minutes.

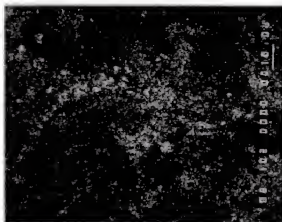


Figure 2-7 Mixed (hydr)oxide coating, Elemental Microprobe scan for aluminum.



Figure 2-8 Mixed (hydr)oxide coating, Elemental Microprobe scan for iron. The picture was also similar to the micrograph of the iron (hydr)oxide surface after attritioning.

Figures 2-7 and 2-8 suggested that the rapid loss of coating from the Ottawa sand surface is indeed a parameter of concern in any application requiring long-term performance.

Additional analysis of an aluminum (hydr)oxide coated collector media exposed to municipal wastewater flow at a superficial velocity of  $80 \text{ L/min m}^2$  again highlighted the problem (see Figure 2-9). The zeta potential curve suggested a rapid loss of aluminum coating from the surface up until day 15. The surface did however remain slightly less negative than the uncoated Ottawa sand and has been shown to capture more microorganisms than the uncoated Ottawa sand [Che98].

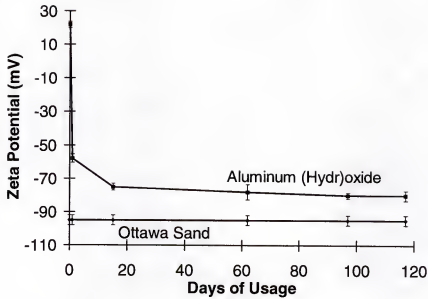


Figure 2-9 Zeta potential values for aluminum (hydr)oxide coated Ottawa sand as a function of multiple days of chlorinated wastewater exposure. Precipitated media treated with non-chlorinated wastewater (not shown) also showed the same apparent loss of charge.

This coating, however, no longer represented a surface capable of “optimal” particle removal. For the specific connotation relating to the use of “optimal” and a discussion on the economic feasibility of using these coating in commercial wastewater filtration please see Appendix C.

This streaming potential application can also be used to monitor biofilm mediated charge effects in addition to granular surface coating stability. In one particular study, a packed column of aluminum (hydr)oxide coated Ottawa sand was exposed to non-chlorinated municipal wastewater for several months under column flow-through conditions. The filtration column was periodically backwashed and samples were taken and rinsed in a sieve tray to remove any non-irreversibly adhered biomaterials. The streaming potential was then used to monitor the surface potential of the granular material

as a function of non-chlorinated water exposure (Figure 2-10). The initial drop observed in the zeta character of the coated media between day 0 and day 15 appeared to be due to the loss of loosely adhered positively charged precipitated metal coating. These results paralleled the results previously shown data for the chlorinated system, Figure 2-10. The packed media after day 15 was then observed to undergo conditioning and biofilm growth [Che98]. In this later stage, day 62 and day 117, the zeta curves indicated a decrease in negative charge as the surface appeared to take on the charge character of the microbes in the biofilm. The zeta potentials of several individual microorganisms common to biofilm having been reported to range from -10 mV to -60 mV [Ach94, Nic93, Vit91]. These

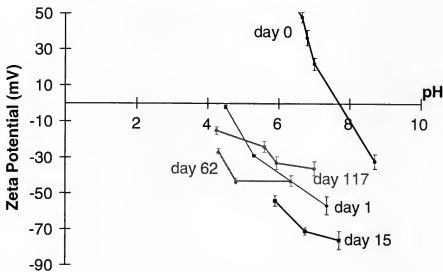


Figure 2-10 Zeta potential curves for aluminum (hydr)oxide coated Ottawa sand as a function of pH and daily continual exposure to non-chlorinated wastewater. Two distinct streaming potential observations are highlighted here, the first being the monitoring of coating stability (the loss of positive zeta character from startup to day 15), the second being the change in zeta values due to the gradual onset of biofilm (the lessening of the negative zeta potential after day 15).

results illustrate the usefulness of this technique to monitor not only the coating stability of the metal (hydr)oxide used in this study but also how biofilm development effects the granular surface's zeta potential and the ensuing particle attachment.

## CHAPTER 3 MICROORGANISM CHARACTERISTICS AND ELECTROKINETICS

### 3-1 General Background on Microorganisms

Bacteria are typically classified into two distinct groups as defined by their reaction to Gram staining. As shown in Figure 3-1B, Gram positive bacteria generally have cell walls composed largely of peptidoglycan ranging from 20 to 40 nm thick [Gie98]. These microbes have non-patterned surfaces that are smooth or slightly rough in appearance. Teichoic acids make up 50% of the total mass of the bacterial cell wall [Gie98] of these organisms and play a large role in defining the surface charge of the Gram positive microbes [Fre79]. *Streptococcus faecalis* (ATCC 19433) and *Staphylococcus aureus* (ATCC 12600) were the Gram positive bacteria chosen for experimentation in this dissertation.

Gram negative microbial species, as shown in Figure 3-1A, have cell walls somewhat thinner than Gram positive bacteria and have a peptidoglycan layer 3 to 8 nm thick followed by an outer membrane which ranges between 6 and 10 nm in thickness. This outer membrane is essentially made up of phospholipid proteins and often has a rough appearance. Occurring as part of the outer membrane are the lipopolysaccharides. These lipopolysaccharides represent the major surface antigenic component, the somatic O antigens. These high molecular weight complexes may be regarded to have 3 regions including a lipid portion (lipid A), a core polysaccharide and finally a specific

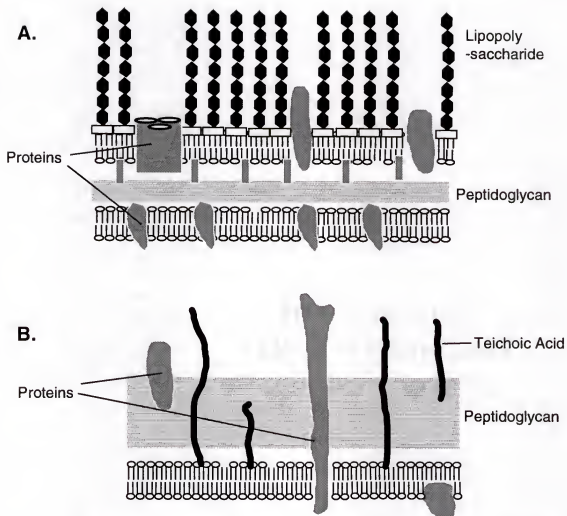


Figure 3-1 Diagram A shows a section of Gram negative bacterial cell wall. Diagram B shows a cell wall section for a Gram positive microbe.



polysaccharide region (the o-specific chains). The o-specific chains are thought to project from the surface of the outer membrane and protect the surface from chemical attack. Other surface appendages such as fimbriae (pili) also commonly extend from the surface with lengths of 0.3 to 1.0 microns. Flagella extend from the surface to distances of 1.0 to 5.0 microns. Many of these microorganisms are also motile. *Salmonella typhimurium* (ATCC 19585) and *Escherichia coli* C3000 (ATCC 15597) were the Gram negative bacteria used in the subsequent research. Scanning Electron Microscopy images of all four of the aforementioned microorganisms are shown in Figure 3-3.

### 3-2 Bacterial Electrostatics

In order to predict potential energy curves for specific collectors and microorganisms, surface potential must be approximated with the use of an electrokinetic technique. Electrophoresis is commonly used in this determination of microbial zeta potentials, which in turn can be used in the approximation of the surface potential on the bacteria. In electrophoresis a sample of fine particles in suspension is subjected to an electrical field. The direction of the particle migration indicates the sign of the charge while the velocity of the particle migration is related to the electrophoretic mobility. In the Brookhaven ZetaPlus instrumentation (Holtsville, NY) used in this work, a laser signal is scattered by the particles moving within the electrical field. This scattered beam is then mixed with a reference beam at the detector which consists of a photomultiplier tube. The reference beam is modulated and the frequency shift of scattered light from a charged particle moving in an electric field ( $w$ ) provides the desired information of both

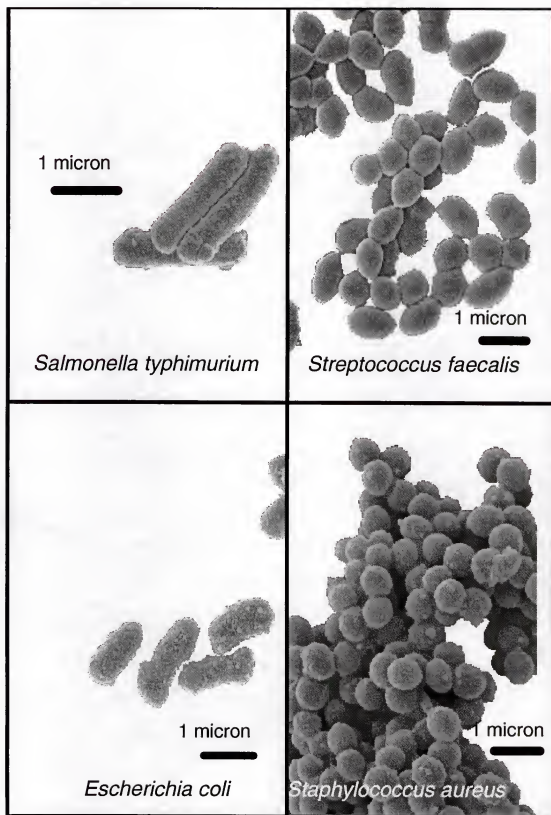


Figure 3-2 SEM micrographs of the four microorganisms used within this study

sign and magnitude. The particle's electrophoretic mobility can be calculated as:

$$w = \mathbf{q} \cdot \mathbf{V}_s = q V_s \cos \phi \quad (3.1)$$

where  $\mathbf{q}$  is the scattering vector,  $\mathbf{V}_s$  is the velocity vector of the moving particle in response to an applied electric field  $E$  and  $\phi$  is the angle between  $\mathbf{q}$  and  $\mathbf{V}_s$ , where

$$\mathbf{V}_s = \mu_e \mathbf{E} \quad (3.2)$$

relates the particle velocity to the electrophoretic mobility  $\mu_e$ . The magnitude of  $\mathbf{q}$  is given by,

$$q = \left( \frac{4\pi n}{\lambda} \right) \sin\left(\frac{\theta}{2}\right) \quad (3.3)$$

where  $\theta$  is the scattering angle,  $n$  is the refractive index of the sample media,  $\lambda$  is the laser wavelength in a vacuum. Zeta potential can then be calculated from the measured electrophoretic mobility as:

$$\zeta = \frac{\mu_e \eta}{\epsilon_0 \epsilon_r} \quad (3.4)$$

where  $\zeta$  represent zeta potential,  $\eta$  is viscosity of the sample,  $\epsilon_0$  is the permittivity of free space and  $\epsilon_r$  is the relative permittivity of the liquid. This equation is based on several assumptions: 1) particle surface charge is uniform and stable; 2) the viscosity, dielectric constant and conductivity in proximity of the particle surface is the same as found within the bulk aqueous media; 3) particle surface is nonconducting; 4) the particle radius of curvature is larger than the Debye screening length [van97a]. These assumptions may fail for bacteria which implies electrophoretic mobility may not accurately convert to zeta potentials via Equation 3.4.

Bacterial surface charge was determined by suspending the microorganisms in distilled water. The bacteria were centrifuged, rinsed and resuspended twice before final

analysis. The resulting microbial zeta potentials as calculated from electrophoretic mobilities are shown in Figure 3-3. The bacterial suspensions were run within a few hours of preparation and no significant bacterial die-off was observed during the course of the zeta potential studies as noted by microscopic observations and bacterial plating. It has been shown that non-living bacteria exhibit a much lower electrophoretic mobility and thus lower zeta potentials [Ada95].

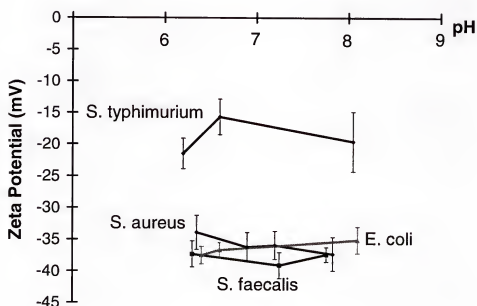


Figure 3-3 Zeta potentials as calculated from electrophoretic mobility data for four microbes at 0.1 mM KCl. Lines are present to clarify data relationships.

Ionic strength of the solution surrounding the bacteria may also effect the number of ions within the electrical double layer, thus altering the bacterial zeta potential. Figure 3-4 shows the effect of ionic concentration on the pH - zeta curves of *S. aureus*. As the KCl concentration increases, the zeta potential curves become less negative. This can be explained by K<sup>+</sup> ions associating within the Stern and shear planes of the microbial

electrical double layer (see section 2-2). The addition of electrolyte shrinks the electric double layer effectively reducing the overall range of the double layer repulsion.

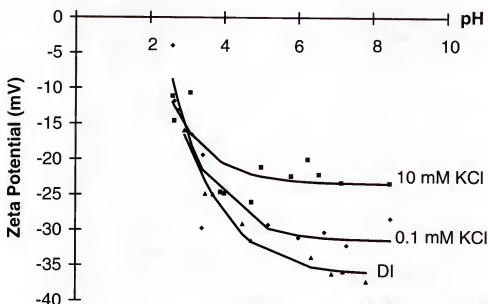


Figure 3-4 Electrophoretically determined zeta potentials for *S. aureus* as a function of aqueous solution ionic strength. Each data point shown above is based on two samples and 6 replicated electrophoretic measurements of those samples. Lines represent an exponential curve fit of the data. DI (deionized water) values correspond to an equivalent 0.05 mM KCl solution assuming only monovalent impurities are present within the water.

Electrophoresis measurements are commonly performed on bacteria to characterize the electrical double layer. Several recent papers have, however, suggested that electrophoretic mobility is influenced by double layer polarization [Duk74, O'Br81, Fix83], a phenomena also known as *surface conductance*. For particles with relatively high surface charge densities (corresponding surface potentials of approximately  $\pm 25$  mV or larger) surface conductance results in a reduction of the electrophoretic mobility. The Helmholtz- Smoluchowski equation (3.4), used to convert electrophoretic mobility to zeta potential, does not account for this retardation and, in effect, under estimates the zeta

potential. This under estimation has been reported to be as large as a factor of two to three [van97a, van97b]. Recent attempts to account for this mobile charge within the bacterial cell wall rely on a combination of techniques which include titration and conductivity measurements [van96, van97a, van97b]. Although the absolute validity of titration procedures to determine surface charge have been questioned [Nre89], surface conduction should be considered when calculating zeta potentials. The values reported within this dissertation should be considered as lower bounds to the surface potentials needed for the theoretical predictions.

## CHAPTER 4

### EVALUATION OF DLVO THEORY THROUGH SIMPLE BACTERIAL DEPOSITION STUDIES

#### 4-1 Introduction

The aim of this study was to investigate the importance of surface potential in microbial deposition to granular surfaces. Recent experimental and theoretical work has indicated that surfaces coated with metal oxides and hydroxide rich oxide/hydroxide mixtures ((hydr)oxides) have the potential to increase the capture efficiencies of commercial filtration systems. This study quantitatively compares different metal (hydr)oxide coatings in their abilities to enhance bacterial deposition. Specifically, the deposition rates of bacterial strains *Streptococcus faecalis*, *Staphylococcus aureus*, *Salmonella typhimurium* and *Escherichia coli*, are compared for Ottawa sand and surface coatings consisting of aluminum (hydr)oxide, iron (hydr)oxide and mixed iron and aluminum (hydr)oxide. The metal (hydr)oxide modified granular media were observed to enhance bacterial deposition relative to the non-coated Ottawa sand. The electropositive surfaces, the aluminum and the mixed hydroxides, had similar average kinetic rate constants five times larger than the rate constants observed for the untreated Ottawa sand. The measured kinetic rate constants for the positively charged systems of aluminum (hydr)oxide and mixed (hydr)oxide collectors suggested that the overall rate of deposition was limited by the transport of the bacteria to the granular surface rather than the rate of attachment. For systems where the collector surfaces were negatively charged, as in the

cases of the Ottawa sand and the iron (hydr)oxide, large energy barriers to attachment were predicted from DLVO theory, but these barriers did not totally inhibit bacterial deposition. Additional comparisons of individual bacterial species deposition behavior also suggested the importance of additional non-DLVO interactions in bacterial deposition. These results were, however, somewhat ambiguous and demonstrated the difficulties of interpreting deposition measurement in terms of particle-surface interactions.

## 4-2 Preparation and Characterization of Surfaces

### 4-2-1 Granular Surface Preparation

The coating procedure of the Ottawa sand has been described in Chapter 2-4. The actual crystal structures produced in these reactions were expected to contain the polymorphs of  $\text{FeO}(\text{OH})$  and  $\text{Al}(\text{OH})_3$  and possibly some of the respective oxides and have been denoted as (hydr)oxides. Again, the expected dominance of the metal hydroxide polymorphs in the coating were expected to provide enhanced deposition over the pure metal oxides of both iron and aluminum as well as the unmodified  $\text{SiO}_2$  (Ottawa sand) [Hie96, Par65] (see Appendix B).

All samples were subjected to pre-attritioning on a vertical 70 cm diameter spinning wheel at 30 rev/min for thirty minutes to remove any loosely adhered surface precipitates. These weakly adhered metallic flocs were removed in order to ensure the validity of the batch deposition studies without removal of additional bacteria through an independent mechanism of flocculation. Coating solubility was not expected to be a



significant factor in these studies due to the relatively low solubility of the aluminum and iron species [Bae76] (Figure 4-1).

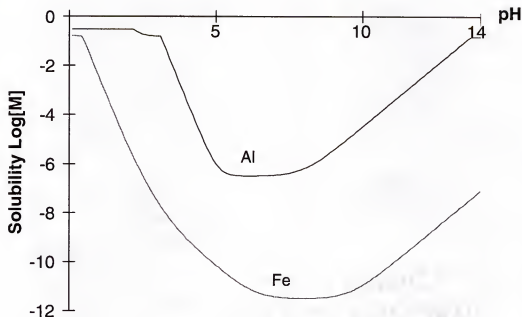


Figure 4-1 Set of solubility curves for both the aluminum and iron species in water [Kra97].

#### 4-2-2 Granular Surface Characterization

The zeta potential of the granular collector media was determined using a streaming potential apparatus as described in Chapter 2. Due to the low electrolyte concentrations used in these measurements, the zeta potential was assumed to be very close to the surface potential and was the value used in the DLVO calculations, although the reader is reminded of the complications surrounding this assumption (see Section 1-3-1).

Induced coupled plasma analysis (ICP) was also run to quantify the concentration of iron and aluminum present on the collector's surface for both modified and unmodified

Ottawa sand. A quantity of 10 grams of collector material was digested in 25 ml of aqua regia (1:2:2::HCl:HNO<sub>3</sub>:H<sub>2</sub>O) for 20 minutes. The solution was heated to a near boil, diluted to 1000 ml and filtered through a 0.2 micron pore size filter prior to ICP analysis. The pH of the dilute solution should be relatively neutral in order to prevent damage to the ICP instrumentation. The diluted samples were then run in triplicate for all four collector surfaces before and after the deposition experiments to test for the loss of iron and aluminum.

Surface area measurements were performed with a Quantachrome NOVA 1200 apparatus. Due to the rather large sizes of the studied granular media (~0.7 mm diameter) a large calibrated cell capable of holding around 8 grams of granular material was used in a 14 point BET adsorption analysis. Specific surface areas were based upon 4 repeated measurements and a correlation coefficient generally greater than 0.99.

Energy Dispersive Spectroscopy (EDS) was used to ensure that no impurities other than aluminum and iron were present on the sand surface. In addition, Scanning Electron Microscope Elemental Microprobe (SEM-EDS) analysis was used to examine the relative surface density and uniformity of the metal species on all four of the collector surfaces. The technique also allowed for the determination of the charge heterogeneity on each surface.

#### 4-2-3 Bacterial Preparation

*Streptococcus faecalis* (ATCC 19433), *Staphylococcus aureus* (ATCC 12600), *Salmonella typhimurium* (ATCC 19585) and *Escherichia coli* C3000 (ATCC 15597) were each grown in 3% tryptic soy broth overnight at 37 °C. *E. coli* and *S. typhimurium* are

cylindrical, motile, gram-negative species, whereas *S. aureus* and *S. faecalis* are spherical, non-motile and gram-positive. The bacteria were centrifuged, rinsed and resuspended in distilled water twice before surface potential and deposition measurements. All samples were used within 1 hour of preparation and no osmotic lysis was observed.

#### 4-2-4 Bacterial Surface Potential

The zeta potential measurements for these bacteria were carried out with a Brookhaven Instrument's Zetaplus model v3.21 zeta potential analyzer (Holtsville, NY). Each sample was pre-rinsed as previously stated and diluted from concentrated bacterial cultures (about  $10^8$  to  $10^9$  CFU/ml) into pH controlled distilled water in a volume ratio of 18:1 water to bacteria. The final concentration of bacteria in water used in the analysis was typically around  $10^7$  CFU/ml.

Distilled water was chosen to minimize charge shielding within the electrical double layer and strengthen the assumed relationship between surface potential and zeta potential. Measurements of zeta potential in ionic and organic buffers have shown significant alteration in the electrical double layer of the bacterial surface [Ada95].

#### 4-3 Deposition Measurements

The deposition studies of the four selected bacteria were carried out under batch conditions at 25 °C. The pH was manipulated to 7.0 with weak KOH additions and the resulting electrolyte concentration was determined to be  $1.1 \times 10^{-5}$  M. An 8 ml volume of  $\sim 10^5$  CFU/ml bacteria solution at pH 7.0 was then added to a number of pre-sterilized

polypropylene 50 ml conical tubes each containing 5 grams of sand. The samples were then placed horizontally onto a New Brunswick orbital shaker table and gently agitated at a speed of 120 rounds per minute. The supernatant was sampled at various times and diluted ten fold in tryptic soy broth (DIFCO Laboratory Inc., Detroit Michigan) before spread plating. The bacterial deposition was determined after plating through the comparison of the number of culture forming units observed for the supernatant at time ( $t$ ) with the bacterial number observed for the control samples ( $C_o$ ). No significant bacterial deposition was observed due to contact with the polypropylene walls of the conical tubes as shown through deposition measurement without the granular media present.

To quantify this rate of particle attachment from the experimental deposition studies, a first order kinetic model was used to fit the data. It was initially assumed that the adsorption process observed within these deposition studies could be described by a first order kinetic rate constant ( $k$ ) that was taken to be invariable with respect to time and uniform among the bacteria population. This would imply that the rate change of bacteria in the supernatant is,

$$\frac{dC}{dt} = -kC \quad (4.1)$$

where  $C$  represents the concentration of bacteria remaining in the supernatant. In relation to the initial bacterial concentration,  $C_o$ , Eq. (4.1) was then solved to produce,

$$C(t) = C_o e^{-kt} \quad (4.2)$$

Eq. (4.2) was fit to the experimental data using nonlinear regression to estimate fitted parameters  $C_o$  and  $k$ . An example of the data and fitting procedure has been included as Figure 4-2.

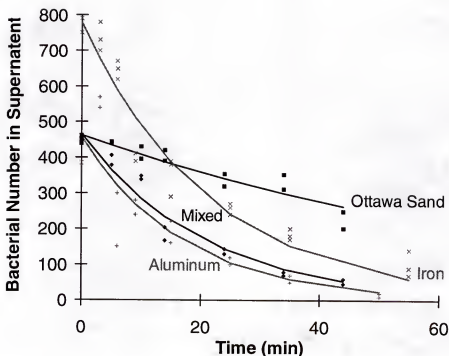


Figure 4-2 Sample set of data representing the number of *E. coli* in the supernatant of the deposition studies as a function of time and exposure to various collector medias.

#### 4-4 DLVO Calculations

The theoretical potential energy of interaction,  $E_{DLVO}$ , between the bacteria and collector was calculated using DLVO theory. A granular collector and bacterium were modeled as a flat plate and sphere, respectively, such that  $E_{DLVO}$  can be written as [Isr92]:

$$E_{DLVO} = E_{vdw} + E_{double} \quad (4.3)$$

where  $E_{vdw}$  is the interaction potential due to van der Waals forces,  $E_{double}$  is the interaction potential due to double layer forces. The van der Waals term ( $E_{vdw}$ ) was determined by,

$$E_{vdw} = \frac{-A_{132}}{6} \left[ \frac{a}{h} + \frac{a}{h+2a} + \ln\left(\frac{h}{h+2a}\right) \right] \quad (4.4)$$

where  $A_{132}$  is the non-retarded Hamaker constant for the system (1: Collector, 2: Water,

3: Bacteria),  $a$  is the radius of the bacteria and  $h$  is surface to surface separation distance between the collector and the bacterium. The diameters of the spherical bacteria and equivalent surface spherical dimensions of the cylindrical bacteria were determined with the aid of UTHSCSA version 1.1 image analysis software and multiple SEM micrographs (Table 4-1). In the determination of the van der Waals component of the energy, the Hamaker constant ( $A_{132}$ ) was calculated with standard non-retarded Lifshitz theory [Isr92] for the various surfaces and bacterial combinations. Literature values were used for the dielectric constants and refractive indices of the granular surface coatings (Table 4-2). A dielectric constant of 78.54, a number reflecting the fact that the bacteria were primarily composed of water, was also assumed for the calculation. (The error associated with this assumption was expected to be very small due to the relative insensitivity of the Hamaker calculation to changes within the dielectric constant.) The bacterial refractive index has been reported to lie within the range of 1.5 to 1.6 [Isr92] and a value of 1.55 was used to represent each of the four bacteria in the Hamaker constant calculations (Table 4-3). Hamaker constant values were within the expected ranges typically predicted for the corresponding oxide surfaces  $1.7$  to  $4.2 \times 10^{-20}$  [Ros88].

Table 4-1 Bacterial properties used in the calculation of DLVO energy curves

Bacteria	Diameters*	(95% CI)	Surface Potential	
			(pH=7.0)	(95% CI)
<i>E. coli</i>	$8.82 \times 10^{-7}$ m	$2.8 \times 10^{-8}$ m	-36.5 mV	$\pm 2$ mV
<i>S. typhimurium</i>	$8.73 \times 10^{-7}$ m	$4.0 \times 10^{-8}$ m	-17 mV	$\pm 1$ mV
<i>S. aureus</i>	$5.89 \times 10^{-7}$ m	$9.0 \times 10^{-9}$ m	-36 mV	$\pm 1$ mV
<i>S. faecalis</i>	$6.39 \times 10^{-7}$ m	$1.3 \times 10^{-8}$ m	-38.5 mV	$\pm 1.5$ mV

\*Equivalent surface spherical diameters of the cylindrical bacteria (*E. coli* and *S. typhimurium*) were determined through the initial calculation of the cylindrical surface area. This surface area value was then assumed to correspond to a spherical particle and the respective bacterial surface spherical diameters were calculated.

Table 4-2 Values used in the calculation of the bacterial Hamaker constant [Isr92]

Material	Dielectric Constant	Refractive Index	Material	Dielectric Constant	Refractive Index
Ottawa Sand*	3.8	1.45	Al <sub>2</sub> O <sub>3</sub> /Fe <sub>2</sub> O <sub>4</sub> Mix	12.45	1.82
Al <sub>2</sub> O <sub>3</sub>	11.6	1.75	H <sub>2</sub> O	78.54	1.33
Fe <sub>2</sub> O <sub>4</sub>	14.2	1.97	Bacteria	78.54	1.55

\* Taken as Quartz

Table 4-3 Granular collector surface properties and respective Hamaker values

Granular Surface	Surface Potential		Hamaker Constant	Surface Area
	(pH 7.0)	(95% C.I.)		
Mixed (hydr)oxide	+35 mV	$\pm 2$ mV	$2.53 \times 10^{-20}$	0.35 m <sup>2</sup> /g
Iron (hydr)oxide	-50 mV	$\pm 2$ mV	$3.22 \times 10^{-20}$	0.32 m <sup>2</sup> /g
Aluminum (hydr)oxide	+22 mV	$\pm 3$ mV	$2.20 \times 10^{-20}$	0.26 m <sup>2</sup> /g
Ottawa Sand	-90 mV	$\pm 6$ mV	$6.60 \times 10^{-21}$	0.46 m <sup>2</sup> /g

The double layer potential was given by an adapted Hogg-Healy-Fuerstenau expression for a sphere-flat plate system [Hog66],

$$E_{\text{double}} = 2\pi a n_{\infty} k_B T \frac{\Phi_1^2 + \Phi_2^2}{\kappa^2} \left[ \frac{2\Phi_1 \Phi_2}{\Phi_1^2 + \Phi_2^2} \ln \left( \frac{1 + e^{-\kappa h}}{1 - e^{-\kappa h}} \right) - (\ln 1 - e^{-2\kappa h}) \right] \quad (4.5a)$$

$$\Phi_i = \frac{ze\phi_i}{k_B T} \quad (4.5b)$$

$$\kappa = \left( \frac{e^2 \sum n_{i\infty} z_i^2}{\epsilon \epsilon_0 k_B T} \right)^{\frac{1}{2}} \quad (4.5c)$$

where  $\phi$  is bulk number density of ions in solution,  $k_B$  is Boltzmann's constant,  $T$  is absolute temperature,  $\Phi_i$  is the reduced potential of either the collector or bacteria,  $\phi_i$  is surface potential as determined by streaming potential or electrophoresis for the collector or bacteria,  $\kappa$  is the reciprocal Debye length,  $e$  is the charge of electron,  $z$  is valence of an ion species. This expression was based upon a constant potential approximation and provided a lower bounds for the predicted energy barriers (these barriers will increase upon incorporation of the constant charge approximation such as the case in charge regulation models [Gra93]). This equation was valid for systems with minimal electrical double layer distortion ( $\kappa a \gg 1$ ) where  $h \ll a$  and for small surface potentials  $\phi$ . Some error was anticipated within the Ottawa sand predictions due to the large negative zeta potential of the collector surface.

#### 4-5 Results

Streaming potential was used to determine zeta potential and charge stability of the four collectors. The preattritioning step showed clear signs that the iron (hydr)oxide was the least stable of the surface precipitates. Despite the higher losses of iron from the coated surfaces during preattritioning, the mixed (hydr)oxide and the aluminum



(hydr)oxide coatings were determined to have positive zeta potentials of statistically different magnitudes. The loss of iron from the iron (hydr)oxide surface resulted in a net negative potential. Zeta potentials of all four collectors have been reported in Table 4-3. Streaming potential measurements on the granular material before and after the deposition experiments showed no changes in zeta potential. In addition, several supernatant samples from the deposition experiments were passed through a 0.25 micron filter and showed no presence of surface coating upon microscopic examination. Additional ICP analysis on the metal content for both the surface coating and the supernatant before and after the deposition experiments again showed no indication of coating loss during the deposition study.

Surface areas were also evaluated for the four collectors in order to rule out the possibility that any observed differences in bacterial deposition could be due to surface area availability. The results (Table 4-3) indicated that the coatings in fact decreased available surface area: Ottawa sand > mixed (hydr)oxide coating  $\geq$  iron (hydr)oxide coating > aluminum (hydr)oxide coating. The loss of surface area upon coating did not appear to justify the observed depositional trends.

EDS was used in the preliminary evaluation of the Ottawa sand surface and indicated a presence of iron and aluminum impurities. No other substantial elemental quantities were observed within the Ottawa sand substrate. SEMEM analysis of the Ottawa sand surface indicated that naturally occurring aluminum deposits were uniformly distributed over the surface. The iron deposits were, however, found as patches on the surface (Fig. 4-3 & 4-4) in low occurrence. The SEMEM signal was determined not to be due to the topological character of the collector surfaces. Under further magnification,



Figure 4-3 SEM-EDS iron map of Ottawa sand surface (white bar represents 10 microns).



Figure 4-4 SEM-EDS iron map of Ottawa sand surface emphasizing the size of these patchwise impurities (white bar represents 1 micron).

these patches of higher iron character were shown to be on the order of several square microns in area (Fig. 4-4) as compared to the 0.3 to 1.0 square micron areas of the microorganisms studied. The frequency of these metallic patches were observed to dramatically increase upon application of the metal (hydr)oxide coatings. A micrograph of an aluminum (hydr)oxide treated surface has been included as Figure 4-5.

Electrophoresis was used to determine the zeta potential of the four bacterial species (see Chapter 3). The technique indicated that the zeta potential of three of the four strains were statistically similar. The *S. typhimurium* was the exception of the four microbes and was found to have a weaker negative potential than the others (Table 4-1). Again, all measurements were taken at pH 7.0.

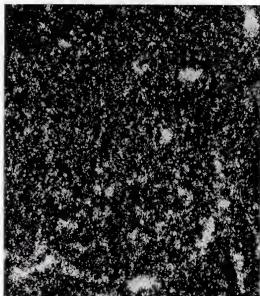


Figure 4-5 SEM-EDS aluminum map of an aluminum (hydr)oxide coated Ottawa sand surface showing the regularly observed patchwise surface impurities (area shown is 13 x 12 microns).

#### 4-5-1 Deposition Results

The bacterial deposition data was modeled as a first order process (4.2) and characterized with corresponding first order kinetic rate constants. The model was observed to adequately fit the deposition data as shown in Figure 4-2. The resulting kinetic rate constants, shown in Figure 4-6, indicated a statistically significant increase in the removal of microbes for the metal (hydr)oxide surface coatings. The electropositive surfaces (aluminum and mixed iron/aluminum coatings) showed the largest kinetic rate constant values and indicated the highest deposition efficiency. In addition, the average kinetic rate constants observed for the aluminum (hydr)oxide and the mixed (hydr)oxide were statistically similar as  $k = 0.0604 \pm 0.006 \text{ min}^{-1}$  and  $k = 0.0650 \pm 0.006 \text{ min}^{-1}$  respectively, suggesting bacterial deposition to be transport limited in the case of these two coatings. These two electropositive coatings had an average kinetic rate constant 1.5 times larger than what was observed for the iron (hydr)oxide coating and were 5 times

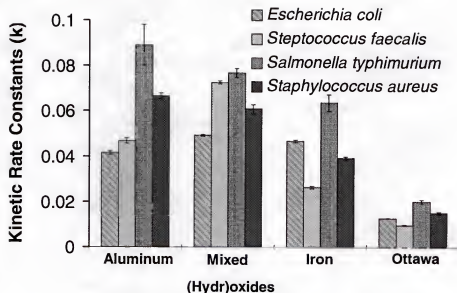


Figure 4-6 Comparison of the kinetic rate constant of deposition as determined with deposition studies.

larger than the rate constant values observed for the untreated Ottawa sand. Even the iron coated media with a zeta potential of -50 mV (40 mV more positive than the uncoated Ottawa sand) showed rate constants on the average 3.5 times greater than the constants seen for the Ottawa sand media.

#### 4-5-2 DLVO Predictions

Systems of interacting negative charges, such as observed for Ottawa sand and iron (hydr)oxide deposition systems (Figure 2-6, pH=7.0), were expected to have a large energy barrier limiting particle attachment. For large energy barriers, the attachment rate constant ( $k$ ) was expected to decrease [Pri76, Spi73]. The DLVO predicted curves for the iron and Ottawa sand systems are shown in Figures 4-7 and 4-8. These Helmholtz potential curves predicted very large energy barriers, which should have prevented

bacterial deposition. Deposition on the iron (hydr)oxide coating and Ottawa sand appeared to be somewhat inconsistent with this theoretical prediction based on detectable depositional rate constants for these two systems in spite of the resulting energy barriers on the order of several hundred to several thousand kT. Because the deposition rate was expected to decrease approximately exponentially with the height of the energy barrier over kT, it would have been very unlikely that the bacteria of this study would have had the necessary energy by thermal fluctuations to transverse the large predicted energy barriers. In addition, the theory as shown in Figures 4-7 and 4-8 suggested that if the attachment rate constants were influenced by double layer and van der Waals forces, in spite of the large energy barriers, removal should follow the order: *S. typhimurium* > *S. aureus* > *S. faecalis* > *E. coli*, in both the Ottawa sand and iron coated systems. However, the measured rate constants for the iron and the Ottawa sand system followed the trend: *S. typhimurium* > *E. coli* > *S. aureus* > *S. faecalis* (Figure 4-6). This disagreement also suggested the importance of other non-DLVO parameters in bacterial deposition particularly between the Gram negative and Gram positive microbial species.

DLVO theory did however, correctly predict the qualitative deposition trend between the collector media as previously mentioned in Section 1-3. As expected, the collector surfaces with positive surface potentials (aluminum and mixed (hydr)oxides) removed more bacteria than the negative counterparts (iron (hydr)oxide and uncoated Ottawa sand).

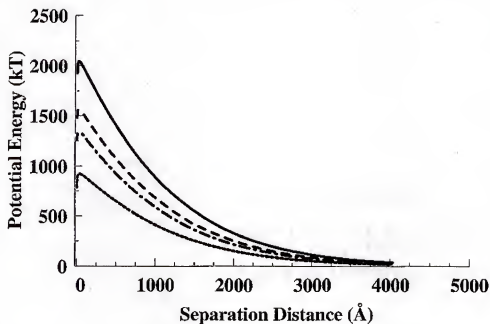


Figure 4-7 DLVO energies (constant potential approximation) as a function of particle separation and type of microbe for non-coated Ottawa sand. *E. coli* (solid line) shows the largest energy barrier, followed by *S. faecalis* (large-dashed line), then *S. aureus* (dash-dot line) and finally *S. typhimurium* (small-dashed line).

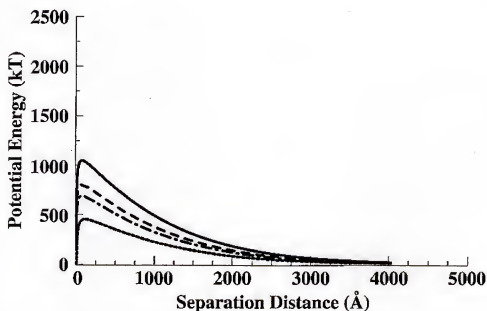


Figure 4-8 DLVO energies (constant potential approximation) as a function of particle separation and type of microbe for iron (hydr)oxide coated Ottawa sand. *E. coli* (solid line) shows the largest energy barrier, followed by *S. faecalis* (large-dashed line), then *S. aureus* (dash-dot line) and finally *S. typhimurium* (small-dashed line).

#### 4-6 Discussion

For positively charged surfaces coated with mixed (hydr)oxide and aluminum (hydr)oxide coatings, DLVO theory predicted negligible energy barriers and thus transport-limited particle attachment [Gre80]. Figure 4-6 in fact suggests this behavior for the aluminum and mixed (hydr)oxides. A comparison of the average rate constants for bacterial deposition between the two positive collector surfaces showed that the aluminum (hydr)oxide and the mixed (hydr)oxide had similar attachment rate constants on average 1.5 times larger than what was observed for the iron (hydr)oxide coating and 5 times larger than the rate constants observed for the untreated Ottawa sand. These results suggested the possibility for substantial improvement of microbe capture through the removal of the interaction energy barrier between the particle via the minimization of the double layer repulsion.

For the negatively charged Ottawa sand and iron (hydr)oxide (after attritioning) surfaces, the reduced attachment rate constants relative to those of the positively charged surfaces were consistent with DLVO theory as a result of the predicted energy barrier to attachment. However, significant bacterial deposition was observed, inconsistent with the very large energy barriers predicted by DLVO theory. The failure of the theory to predict microbial attachment kinetics has been reported by several other researchers for various systems [Ver48, Der41, Joh96, Eli90]. Previous explanations accounting for this observation have included deposition within a secondary minima, influence of shape factors on particle interactions, polarization of the electrical double layer, collector surface roughness and distributions in surface potential [Eli90]. Of these hypothesis, the most frequently cited explanation has been based upon non-idealities such as cracks,

crevasses and impurities at the granular surface [Isr92, Eli95, Son94, Rya96, Hol97] which in turn have produced surface charge heterogeneities. However, the lower surface area measured for the iron (hydr)oxide surface relative to the Ottawa sand surface suggested a decrease in surface non-idealities. Alternatively, the Ottawa sand was shown via EDS to have positive metal impurities of aluminum and iron on the surface. These metallic impurities could provide favorable sites for particle interaction if present as large patches on the Ottawa sand substrate. Further analysis of the Ottawa sand surface via SEMEM also supported the plausibility of this explanation in accounting for the anomalous deposition. As shown in Figures 4-3 and 4-4, iron deposits were found to be intermittently present on the Ottawa sand surface as patchwise heterogeneities with surface areas of several square microns. The projected area of interaction for a bacteria is on the order of 0.3 to 1.0 square microns. SEMEM analysis also showed the aluminum to be randomly and more uniformly distributed on the Ottawa sand surface. Since the streaming potential measurements indicated that the sand surface had a net negative potential, it would not seem likely that these disperse, uniform distributions of aluminum would have been responsible for producing the favorable sites for microbial deposition. Instead, the patchwise charge heterogeneities caused by the iron impurities would be the more probable sites for deposition within the Ottawa sand system.

The iron (hydr)oxide coated collector surface could also increase bacterial removal utilizing a similar mechanism. The pre-attritioning procedure, as outlined in Section 4-2, resulted in a loss of the iron (hydr)oxide coating from the Ottawa sand surface. The resulting surface was found to have a net negative charge but appeared to be made up of discrete and random distributions of positively charged iron (hydr)oxide. The



overall increased quantity of these positively charged patches relative to the Ottawa sand surface could account for the anomalous bacterial deposition in the iron system despite the existence of the large prohibitive energy barriers predicted by DLVO theory.

The deposition of bacteria onto the net positive collector surfaces would again be in response to the increased statistical probability that a bacteria would find itself in a region of the collector where the localized charge would correspond to an energy barrier less than 10 kT. Figure 4-5 shows a sample SEMEM micrograph of an aluminum (hydr)oxide coated surface demonstrating a clear increase in the number of favorable interaction sites available for particle deposition. The more continuous the aluminum (hydr)oxide or iron (hydr)oxide coatings, the higher probability of particle capture.

Although surface charge heterogeneity may have been the reason behind the observed bulk deposition of bacteria in general for negative collector systems, the removal trends between the bacterial species themselves deserved further consideration. For similarly charged systems of negative particles, this study failed to find a direct correlation between the depositional behavior of the individual microbes, Figure 4-6, and the behavior predicted by the height of the energy barriers calculated by DLVO theory, Figures 4-7 and 4-8. This seemed to indicate that similarities in zeta potential, as seen for *S. faecalis*, *S. aureus* and *E. coli*, had not correspondingly influenced the degree of microbial removal for systems of large energy barriers. In addition, the disagreement between the deposition trends of the diffusionally limited systems (aluminum (hydr)oxide and mixed (hydr)oxide) and the attachment limited systems (Ottawa sand and iron (hydr)oxide) suggested the possible importance of other non-DLVO parameters.

The kinetic deposition data indicated that the Gram negative bacteria

(*S. typhimurium* and *E. coli*) were removed to a greater degree than the Gram positive bacteria in systems with negative collectors. One possible mechanism for the increase in particle attachment may be attributed to the presence of bacterial surface appendages and their potential ability to span the energy barrier and contact the collector's surface. The length of flagella of these Gram negative bacteria typically range from 1 to 5 microns. In addition, fimbriae (pili) generally have a length between 0.3 to 1.0 microns [Fre79]. Such appendages could possibly transverse the predicted DLVO energy barriers of Figures 4-7 and 4-8 while keeping the bacterial membrane at separation distances of 0.3 or 0.4 microns from the collector surface where the energy barriers would be minimal.

Alternatively, these surface appendages may be able to probe along the collector surface and through their random motion find areas of favorable interaction where the energy barrier is less than 10 kT and the bacterial membrane can attach. Such an explanation could account for the particle capture through avoidance of the total height of the interaction energy barrier. Similarly, motility of the Gram negative microbes may also account for this deposition trend to some degree. The ability of the bacteria to move relative to the surface could increase each particles likelihood of finding favorable sites for deposition. Such explanations could account for the apparent higher particle deposition for the Gram negative bacteria relative to the Gram positive.

#### 4-7 Conclusion

This study was performed in an attempt to relate particle adhesion to surface charge through a commonly used deposition approach. The results seemed to support the hypothesis that a repulsive energy barrier was in fact responsible for controlling the

bacterial deposition to the various granular surfaces. These general qualitative observations were also consistent with DLVO predictions. DLVO theory did not, however, quantitatively describe the observed deposition. Surface heterogeneity appeared the most probable reason for the unexpected deposition of both the Gram positive and Gram negative bacteria onto the iron (hydr)oxide collector surface. The anomalous bacterial deposition onto the unmodified Ottawa sand surface was somewhat more difficult to account for since the number of high density iron sites were not as prevalent on the Ottawa sand as found for the modified iron (hydr)oxide surface. In general, these simple deposition experiments appeared to be too insensitive to provide conclusive information for overall applicability of DLVO theory and the relative importance of other interactions potentially involved in bacterial deposition to these surfaces. The difficulty in directly relating surface properties to deposition behavior again highlights the importance of directly measuring interparticle forces, which is the topic of the next chapter.

## CHAPTER 5

### DIRECT MEASUREMENT OF INTERPARTICLE FORCES ON BIOLOGICAL COLLOIDS

#### 5-1 Background on Surface Force Measurements

The realization as to the importance of the direct surface force measurement can be traced back to the first study of particle forces as a function of separation distance by Rayleigh in 1936 [Ray36]. Several attempts to relate particle association to interaction forces have since followed [Cra97]. The theoretical treatment of these interaction forces eventually resulted in the well-known DLVO theory from the work of Derjaguin, Landau, Verwey and Overbeek [Der41, Ver48]. The first attempts to validate this theory through comparison of direct surface force measurements was undertaken several years later by Derjaguin and coworkers [Der64]. Subsequently, many researchers have found good agreement between DLVO predictions and directly measured long range surface forces within systems of non-biological particles and surfaces. This has included work done with quartz utilizing cantilever springs [Pes76], mica cylinders with the Surface Force Apparatus [Isr78] and various combinations of flat plate/colloidal systems using glass, quartz and alumina with the Atomic Force Microscopy [Duc91, Hig97, Kar97]. Equivalent direct measurements of the colloidal forces between a bacterium and planar surfaces as a function of separation distance have not been as successful and have generally relied upon interparticle force measurements between protein coated surfaces [Kle84, Lec93, Fra97, Rob98] and bacterial lawns [Raz98]. Recent attempts to measure

forces between a single bacterium mounted upon an AFM cantilever [Bow98] has served to highlight the difficulty of studying biological interactions with traditional force measurement techniques. The recent combination of evanescent wave light scattering [Che79, Tem81, Pri87] along with three dimensional optical trapping [Ash92] has resulted in a technique capable of measuring the forces between single microorganisms and a glass surface [Cla99]. This technique has been called Three Dimensional Optical Trapping with Evanescent Wave Light Scattering (3DOT-EWLS).

In this study, the 3DOT-EWLS technique was used to measure the long range interaction forces between a single *Staphylococcus aureus* microbe and a glass surface as a function of separation distance. The measurements were performed for three different electrolyte conditions in order to vary the repulsive electrical double layer force. These results were then compared to theoretical predictions of the interaction force as calculated by the Hogg-Healy-Fuerstenau DLVO expression adapted for a sphere/flat plate system [Hog66] as previously described in Chapter 4-4. Such a quantitative comparison should provide insight as to the appropriateness of the DLVO approach in describing systems of microbial interaction.

### 5-2 Quantitative Measurements of Interparticle Forces

*Staphylococcus aureus* (ATCC 12600) was grown in tryptic soy broth overnight at 37 °C. The bacterial suspension was then centrifuged for five minutes at 5000 RPM. The supernatant was then decanted and the microbes were resuspended in distilled water. The procedure was repeated twice and the resulting bacterial suspension (concentration

around  $1 \times 10^8$  CFU/ml) was resuspended in electrolyte solution to a concentration on the order of  $1 \times 10^4$  CFU/ml for 3DOT-EWLS analysis.

### 5-2-1 Three Dimensional Optical Trapping Evanescent Wave Light Scattering Apparatus

The 3DOT-EWLS technique has been described in detail elsewhere [Cla99] and is briefly summarized here. The 3DOT-EWLS device was constructed upon an inverted optical microscope (Diaphot 200, Nikkon, Mellville, N.Y.) and utilized an X-Y motorized stage (LUDL Electronic Products, Hawthorn, N.Y.). Samples were prepared to include the *Staphylococcus aureus* microbes as described above along with 10 micron polystyrene spacer beads (Polysciences, Warrington, PA). A single drop of the sample solution was placed upon a microscope slide (precleaned, used as received from Fisher) and covered with a cover slip. The slide was inverted and pressed upon a paper towel to remove excess solution and compress the sample down to the 10 micron spacer gap. The outer edges of the cover slip were then sealed with silicone stopcock grease to prevent evaporation during analysis. The sample was mounted onto the microscope using immersion oil on the objective lens (see Figure 5-1). A 100mW diode laser (Cell Robotics, Albuquerque, NM) was then focused through a high numerical aperture objective (Plan Fluor 100X, 1.3 numerical aperture; Nikon, Japan) to a spot with diameter on the order of the wavelength of the light. This focused beam created a three dimensional optical trap (3DOT), which allowed for capture and control of particles with a refractive index higher than the surrounding solution by attracting them to the region of highest light intensity [Ash92]. A monochrome CCD camera (Thomas Optical Measuring Systems) was mounted onto one of the microscope eye pieces and allowed for

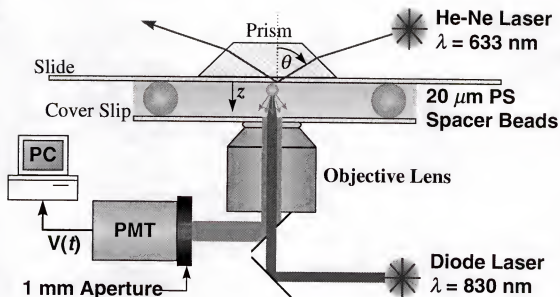


Figure 5-1 Diagram of an inverted microscopy system and additional instrumentation as used by 3DOT-EWLS.

visualization and capture of an individual colloidal particle within the test solution. The generation of the evanescent wave relied upon the total internal reflection of a 17 mW randomly polarized, 632.8 nm, Helium-Neon laser (Melles Griot, Irvine, CA) within a dove prism (BK7 glass, 45 degree angle; Optosigma, Santa Ana, CA). The prism was optically coupled to the inverted microscope slide with a refractive index matching immersion oil ( $n_d = 1.515$ ). As the trapped colloidal particle approached the microscope surface it entered the evanescent wave propagating parallel to the slide surface causing light to be scattered. This scatter was then selectively monitored with the use of a  $633 \text{ nm} \pm 2 \text{ nm}$  band pass filter (Nikon, Japan), a 1 mm aperture and a photomultiplier tube (PMT) (Oriol Instruments, Stanford, CT). The PMT voltage signal was then amplified and sent to a data acquisition board and stored on personal computer for further analysis.

### 5-2-2 Characterization of Interacting 3DOT-EWLS Surfaces

The surface potentials of the glass slides used within this study were estimated from streaming potential measurements as a function of electrolyte concentration. The streaming potential device used for this study was constructed using a Van Wagenen and Andrade design [VanW80]. Atomic Force Microscopy (AFM) was also used to characterize the average roughness of the glass surfaces used in these studies since surface roughness has been reported to affect interparticle forces [Sur97].

*Staphylococcus aureus* is a spherical Gram positive bacteria with a cell wall structure shown in Figure 2-1B. The cell wall consists of an open, loosely-knit structure of proteins and teichoic acids with carboxyl, amine and phosphate groups extending from a polydisaccharide backbone [Fre79]. The zeta potential measurements on the microbes were performed using a Brookhaven Instruments Zetaplus model v3.21 zeta potential analyzer (Holtsville, NY). Each sample was pre-rinsed as previously described and diluted to a final concentration on the order of  $1 \times 10^7$  CFU/ml within pH controlled solutions at various electrolyte concentrations. It should be noted that surface conduction within the microbial cell wall may play a significant role in under predicting microbial zeta potentials as calculated from electrophoretic mobilities with the Helmholtz-Smoluchowski relation [van97a].

### 5-3 Bacteria/Glass Interaction Forces

The ability of the 3DOT-EWLS device to reproducibly measure the forces between an *S. aureus* microbe and a glass slide surface was evaluated for the *S. aureus* - glass system at 0.92 mM KCl. The higher electrolyte values was chosen to be



representative of the most difficult 3DOT-EWLS system studied to date. This was due in part to the increased background scatter generally observed at higher electrolyte concentrations. Three such curves are shown in Figure 5-2 corresponding to two different bacteria interacting with the same area of the glass slide and a third bacteria interacting with a new slide position. This figure shows the characteristically consistent measurements. The reproducibility of the exponential portion of these curves was of particular interest and were further characterized by curve fitting to the equation,  $y=A\exp(Bx)$ . The  $R^2$  value of these curve fits were 0.9 or greater. Statistical analysis of B values (5 in total) yielded a mean value of  $0.054 \text{ nm}^{-1}$  with a standard deviation of  $\pm 0.002 \text{ nm}^{-1}$ . The results suggest a reasonably high degree of reproducibility in the 3DOT-EWLS measurements.

The measurement technique was also applied to *S. aureus* microbes at two additional electrolyte concentrations as indicated in Table 5-1. The increasing electrolyte conditions were expected to alter the electrical double layer repulsion between the bacterium and the glass slide. Figure 5-3 shows both the 3DOT-EWLS force and energy curves for the three measured electrolyte conditions. The addition of KCl resulted in the gradual development of a secondary energy minima and an increase in the rate of observed exponential decay of the repulsive force as a function of separation distance. Both trends are consistent with the behavior predicted by DLVO theory. The curves shown in Figure 5-3 are arbitrarily spaced with respect to one another and their absolute separation distance with the glass. DLVO theory shall be used to approximate possible separation distances of the measured 3DOT-EWLS curves and the corresponding calculations have been included within the next section.

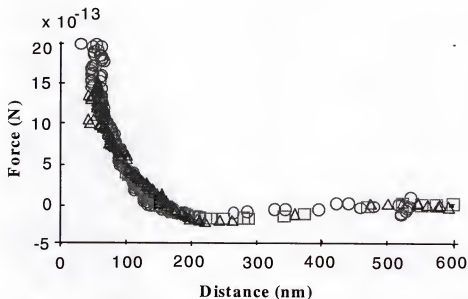


Figure 5-2 Three sample 3DOT-EWLS curves demonstrating the reproducibility of the bacterial force measurement for the *S. aureus* - glass system at 0.921 mM KCl. Data compares two different *S. aureus* microbes at the same position on the glass slide and a third *S. aureus* microbe at a new location.

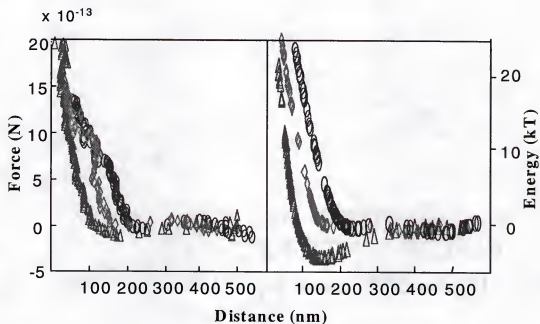


Figure 5-3 3DOT-EWLS curves for *S. aureus* - glass slide system at three different electrolyte concentrations. The open circles represent 0.145 mM KCl, the open diamonds represent 0.454 mM KCl and the open triangles represent 0.921 mM KCl.

#### 5-4 DLVO Theoretical Predictions

The average diameter of the *S. aureus* microbe was measured to be  $0.55 \pm 0.05$  microns with the use of the Brookhaven ZetaPlus instrument. The microbe surfaces were spherical, non-patterned with many polymeric protrusions expected to extend from the cell wall surface [Fre79, vanI84]. Atomic Force Microscopy was used to measure the roughness of the glass slide surface within the 3DOT-EWLS experimentation. The resulting root mean squared roughness was determined to be 0.28 nm with a  $Z_{\max}$  value (distance separating the highest and lowest points on the surface) of 3 nm. Zeta potential values were used to approximate surface potentials within the DLVO calculations and have been included within Table 5-1 as a function of KCl concentration at pH 6.3 and 25°C. Solution ionic strength was calculated from conductivity measurements.

Table 5-1 Properties of interacting 3DOT-EWLS surfaces

	$\eta$	$\epsilon$	Ads. Freq.	Approximated Surface Potential		
				0.145 mM	0.454 mM	0.921 mM
<i>S. aureus</i>	1.5	78	$3.0 \times 10^{15} \text{ sec}^{-1}$	$-32 \pm 3 \text{ mV}$	$-27 \pm 3 \text{ mV}$	$-23 \pm 3 \text{ mV}$
Glass	1.51	4.29	$3.0 \times 10^{15} \text{ sec}^{-1}$	$-44 \pm 3 \text{ mV}$	$-33 \pm 3 \text{ mV}$	$-22 \pm 3 \text{ mV}$
Water	1.33	78	$3.0 \times 10^{15} \text{ sec}^{-1}$			
Debye Lengths:				28 nm	22 nm	11.5 nm

#### 5-5 Comparison of DLVO Theory to 3DOT-EWLS Experimental Data

The van der Waals and double layer repulsion expressions (Eqns. 4.3-4.5) were calculated for the bacterium/glass slide system. The results have been reported in Figure 5-4 in comparison to the 3DOT-EWLS measured data. The values used for the surface charge, dielectric constants [Isr92], refractive indices [Eli95] and absorption frequencies

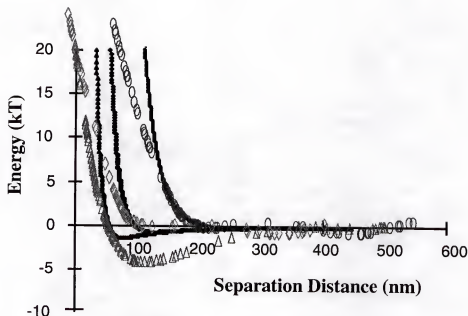


Figure 5-4 Comparison of 3DOT-EWLS data (open symbols) with DLVO predictions (solid symbols). The circles represent 0.145 mM KCl, the diamonds represent 0.454 mM KCl and the triangles represent 0.921 mM KCl. The experimental data appeared to have much larger decay lengths than the theoretically predicted data.

[Isr92] have also been included in Table 5-1. The DLVO predictions were used to estimate absolute separation distance. Initial comparisons between experimental data and the DLVO curves suggested the ability of the theory to describe general qualitative trends within the bacterial systems (see Figure 5-4): the decay lengths were observed to decrease while the depth of the secondary minima grew with increasing electrolyte concentration. On the quantitative scale, the Hamaker constant ( $A_{132}$ ), calculated to be  $0.8 \times 10^{-20}$  J from non-retarded Lifshitz theory, appeared to adequately describe the depth of the secondary minima measured by the 3DOT-EWLS technique for the 0.145 mM and the 0.454 mM curves. In addition, these DLVO curves appeared to match the 3DOT-EWLS data up to energy barrier heights of several kT. The theory matched the 0.145 mM experimental measurements up to values of 10 kT followed by a match of the 0.454 mM data up to

5 kT.

The 0.921 mM data appeared to follow the same trend showing deviation from DLVO theory at energies less than 5 kT. The measured data of this case had a much larger attractive interaction than predicted by theory. The Hamaker value of  $0.8 \times 10^{-20}$  J grossly under predicted the experimentally observed secondary minima. The theory required a more unreasonable Hamaker value around  $1.9 \times 10^{-20}$  J to match the minima depth shown by the 3DOT-EWLS results. Even with this larger than expected value, the overall shape of the minima was poorly matched by the theory. In addition to these observations on the secondary minima, the theoretical curves also appeared to overemphasize the severity of the observed double layer repulsion as fit with the expression  $y = A \exp(Bx)$ . A fact that has resulted in a theoretical under prediction of the decay lengths calculated for all three electrolyte concentrations (see Figure 5-5).

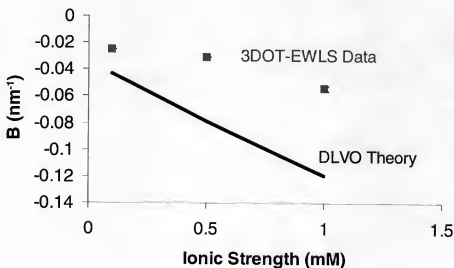


Figure 5-5 Comparison of experimental and theoretical interaction force decay lengths.

## 5-6 Discussion

### 5-6-1 Failure of DLVO Theory to Match 3DOT-EWLS Bacterial Data

The use of DLVO theory to describe interaction forces between relatively simple, well defined surfaces such as glass and mica have been reported to be successful by many authors [Duc91, Duc92, Isr78]. In addition, recent work with 3DOT-EWLS utilizing colloidal silica and a glass slide surface has also demonstrated a similar successful correspondence between the DLVO predictions and the direct force measurements [Cla99]. Studies within systems of biological particles, however, have to date been much more ambiguous. The *S. aureus* cell wall has been shown to consist of loosely knit proteins, acids and other polymeric protrusions [vanI84] all of which are expected influence the van der Waals and double layer forces. In addition, these protrusions may potentially cause non-DLVO type behavior due to bridging, steric and receptor ligand type forces. Although such additional interaction forces have been theorized, conclusive evaluation of the DLVO has not been forthcoming within the literature. Studies reporting anomalous deposition between similarly charged microbes and surfaces have however suggested that the repulsive interaction forces may not be as dominant as predicted by DLVO theory [Eli95, Wal98]. The direct comparison of the 3DOT-EWLS curves to DLVO predictions should help to provide insight into the overall applicability of DLVO theory to microbial systems.

In contrast to earlier work with inorganic colloidal particles, DLVO theory appeared to be relatively unsuccessful in describing the 3DOT-EWLS data curves presented in Figure 5-4. Most notably, the exponential decay of the experimental results did not appear to be as severe as predicted by theory. This deviation could be due to



Table 5-2 Possible explanations accounting for observed deviations between experimental data and theory

Charge Heterogeneity [Elh95, Som98]	Distributions of charge over interacting surfaces lowers height of energy barrier between interacting particles.	Not clear if effect is present in colloidal silica/glass system at low electrolyte [Cla99, Jia93] Distribution of charges necessary to achieve decay lengths reported by 3DOT-EWLS technique require energy barriers on the order of a single kT (in disagreement with Figure 5-4).
Surface Roughness [Elh90]	Surface asperities were calculated to substantially reduce the height of the theoretical energy maxima between surfaces. 1) Roughness effects on vdW force become negligible at separation distances larger than the characteristic size of the roughness ( $r_{\text{bacteria}} < r_{\text{glass}} \sim Z_{\text{max}} \leq 3 \text{ nm}$ ) 2) As asperity height of <i>S. aureus</i> increases, double layer repulsion increases at larger separation distances and energy barrier height increases	Reduction of barrier height would not entirely account for increase in decay lengths reported here.
Surface Roughness [Wal298]		Trend suggested here would serve to decrease the theoretical decay lengths to an even greater extent.
Hydrophobic Interactions [Pas85, vanL87a]	Potential attractive contribution to the force profile due to free energy minimization within a system. Force has been reported to be orders of magnitude greater than vdW forces.	Glass slide surface would not be expected to have hydrophobic sites present.
Dynamic Hamaker	Refractive indices and dielectric properties change as cell wall matrix is compressed. Bacterial Hamaker increases as a function of separation distance and nature of the interaction.	Range of Hamaker values needed to reduce predicted decay lengths would be too large to entirely account for the observed decay lengths. Separation dependent Hamaker approaches also failed.
Receptor-Ligand [Dic97]	A lock and key mechanism requiring specific proteins and ligand.	<i>S. aureus</i> has a receptor although the reciprocating ligand is not expected to be present on the glass slide
Polymeric Bridging [Jon83]	Extension of polymeric surface appendages from a colloidal surface across a restrictive energy barrier which allows for a reduction in overall energy of approach.	Length scale suggested by DLVO fitting of the 3DOT-EWLS data would require bridging of a gap around 150 nm (0.145 mM data).
Deformation of Microbe in Optical Trap	If the <i>S. aureus</i> were to deform during measurement it would do so at the expense of some degree of particle displacement within the optical trap and thus lower the measured energy.	Force exerted here on the microbe within this study was around 2 piconewtons while bacteria are pressurized to values greater than 5 atm [Mad97]. No deformation expected.
Compression of Peptidoglycan and or Surface Appendages	Solution conditions will control the amount of force required to reconfigure the polymeric bacterial projections. Bacterial cell wall thickness can be dependent on salt conc. [Pie95].	Potentially true. More salt, more charge shielding, weaker repulsion between dominant phosphorous groups within bacterial proteins and acids, less force needed to fold membrane polymers on themselves (see Section 5-6-2).



3DOT-EWLS data to negative separation distance prevents the two higher electrolyte curves from being shifted any further to the left.) Other explanations based upon possible variations within the input parameters to the DLVO theory (such as surface charge, Hamaker constant) also failed to account for the overall shift in decay lengths observed between experiment and theory (see Table 5-2).

The apparent lack of an adequate explanation accounting for the observed exponential character of the measured force curves led to the examination of the physical relationship between the microorganism and the 3DOT-EWLS measurement. The optical trap captures a single bacterium and allows for a systematic probing of the interaction forces between the microorganism and the glass surface. During this measurement the microorganism is capable of undergoing displacement from the center of the trap. In addition, compression within the polymeric projections surrounding the cell wall may also occur. If the interaction forces are great enough, deformation of the microorganism's shape (from sphere to oblate spheroid) may even be possible (see Figure 5-7).

Displacement refers to the response of the microbe within the optical trap as it is forced away from the trap center by the interaction forces arising between the microorganism and the glass surface. The potential compression of the loosely-knit cell wall would result in a weakening of this overall displacement force to some degree and thus lower the measured interaction force/energy. Bacterial deformation, however, seems unlikely given that the *S. aureus* has an internal osmotic pressure around 5 atm [Act88]. Calculations of deformation force as based upon osmotic pressure of the bacterium indicate that a 0.25% deformation in bacterial radius would require 1.0 nanoNewton of force. A force greater than the 2 picoNewtons exerted on the microbe during the analysis shown in Figure 5-3.

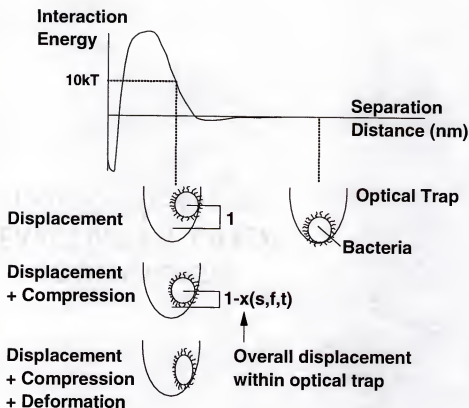


Figure 5-7 Possible bacterial conformations within the 3DOT-EWLS optical trap (represented here as a parabola) during the measurement of particle interaction forces. The compression effect, if present, would serve to lessen the overall displacement of the microorganism within the optical trap by some quantity ( $x$ ) which should be a function of the structural properties of the cell wall polymers ( $s$ ), the force exerted on the cell wall ( $f$ ) and the time over which this force is exerted ( $t$ ).

#### 5-6-2 Compression of the Bacterial Cell Wall

The absence of an explanation to fully account for the experimental deviations recorded by the 3DOT-EWLS technique suggests the importance of bacterial cell wall compression during analysis. The 3DOT-EWLS measurement requires the trapped particle to experience interaction forces over several minutes as the particle displacement within the optical trap is measured as a function of decreasing separation distance (Figure 5-8). The physical properties of the bacterial cell wall would in turn dictate the degree of

compression [Juc98] and the time scale over which the compression is expected to occur. A trend that seems to be supported by the decreased correspondence between the theoretical and experimental curves in Figure 5-4 as a function of electrolyte concentration. To this end, some fraction of the interaction energy may be used to compress the bacterial cell wall instead of purely displacing the particle from the trap center. In natural systems, bacterial exposure to the interaction barrier is on the order of seconds and is dependent upon the Brownian motion of the particle. If cell wall compression is fast relative to the time of the bacterial interaction, then the 3DOT-EWLS curves would be representative of the forces expected between the glass and microbe. If a fraction of the bacterial membrane compression occurs during the natural time scale, then the 3DOT-EWLS interaction curves would represent a lower bounds of the interaction and an under estimation of the true interaction energy curve's exponential decay.

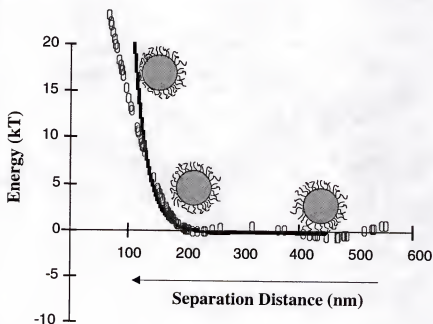


Figure 5-8 Diagram suggesting the reconfirmation of the bacterial membrane/bacterial polymeric projections upon experimental probing of a glass slide surface within the 3DOT-EWLS device.

### 5-6-3 Electrolyte Effects

The addition of electrolyte is expected to lower the double layer repulsion between the two interacting surfaces as well as influence the physical nature of the bacterial cell wall. The wall should have a considerable negative charge present within its polymer matrix at weaker electrolyte concentrations due to the dominance of the phosphate groups in the teichoic acids. More force would therefore be needed to fold these polymer chains back onto themselves or the surrounding chains. As the electrolyte concentration of the solution increases the phosphate charges become shielded and the amount of force necessary to fold these polymeric extensions back onto themselves would be expected to decrease. A fact already evident within the random coiling of the straight chained teichoic acids upon addition of electrolyte [Ber80]. Such an explanation could account for the trend in  $kT$  values at which the experimental curves begin to deviate from the theoretical predictions in Figure 5-4 ( $10\ kT$ ,  $5\ kT$ ,  $< 5\ kT$ , corresponding from weakest to strongest electrolyte concentration). So the amount of force and time for compression may be significantly lower at higher electrolyte concentrations.

### 5-7 Conclusions

The 3DOT-EWLS measured force curves for the spherical *S. aureus* bacterium showed significant deviation when compared to the corresponding DLVO predictions. A stronger attractive force appeared to be present at higher electrolyte concentrations resulting in a larger secondary minima than expected. In addition, the exponential section of the of the energy curve suggested a much larger decay length than predicted by theory in contrast to previous work done on colloidal silica in which the DLVO theory

successfully matched 3DOT-EWLS data [Cla99]. The deviations between the measurements and the theoretical predictions suggest the possible importance of bacterial cell wall compression during course of the 3DOT-EWLS measurement. Future work needs to be directed towards understanding the time scale over which this compression occurs in order to evaluate how representative the 3DOT-EWLS measurements are of naturally occurring bacterial interactions.

## CHAPTER 6

### FEASIBILITY OF CHEMICAL MODIFICATIONS WITHIN THREE DIMENSIONAL OPTICAL TRAPPING EVANESCENT WAVE LIGHT SCATTERING STUDIES

#### 6-1 Introduction

Although the relationship between particle-surface interactions and surface modifications may not be instantly recognized, there exists a need for well defined, fully characterized, systematically modified surfaces in fundamental particle interaction studies. Various forms of surface heterogeneities have historically limited the success of attempts to link surface forces and physical properties. Uniform surface modifications would have potential for use within the newly developed 3DOT-EWLS system. Surface modifications of the 3DOT-EWLS glass test surfaces could allow for selectively engineered glass surfaces with a variety of hydrophobic structures, surface charges, ligand binding sites and surface roughnesses beyond those allowed by a simple glass surface. Such modifications to the EWLS glass would be limited by optical transparency, uniformity and stability in aqueous environments. Silane compounds were subsequently considered for this task in an attempt to take advantage of the covalent nature of the silane bond and the large number of functional silanes available for commercial usage.

## 6-2 Materials and Methods

### 6-2-1 Silane Surface Preparation

The majority of the silanated glass surfaces were prepared through the use of a 95% ethanol, 5% water solution to which the silane was added to reach a 2% final concentration. Five minutes were then allowed for silane hydrolysis and condensation within the bulk aqueous medium (Figure 6-1). The glass slides were then dipped into the solution and removed after 2 minutes. The polymerized silane of the condensation phase was expected to deposit onto the glass in a random fashion producing a loose interconnected multilayer network of chemisorbed and physisorbed silanes [Ark77]. These surfaces were then rinsed twice with ethanol and allowed to cure at room temperature for 24 hours [Mit92, Plu82]. The cured surfaces were made of multilayered silanes [Ark77, Moo97, Goo90] in which the thickness of the silane was determined by initial concentration within solution [Ark77].

The more complex N,N-dimethylbutylamine (N,N-DMBA) surface coating involved three reactions as described by Suhara et al. [Suh95]. During the first reaction, acid washed glass was exposed to 0.5 ml of 2,4,6,8-Tetramethylcyclotetrasiloxane (TMCTS). The glass was then heated to 80 °C in a sealed container for 10 hours followed by an additional 20 hours in an open container. The poly-TMCTS coated surfaces were rinsed with toluene and refluxed at 110°C for 6 hours in 500 milliliters of toluene, 0.05 mg of chloroplatinic(IV) acid hexahydrate, 0.05 mg of tributylamine and 5 milliliters of chloromethylstyrene. The glass surfaces were again rinsed with toluene and allowed to dry under vacuum. In the third and final reaction, the reacted glass, 50 milliliters of N,N-DMBA and 500 milliliters of acetonitrile were heated at 65 °C for 4 hrs. This

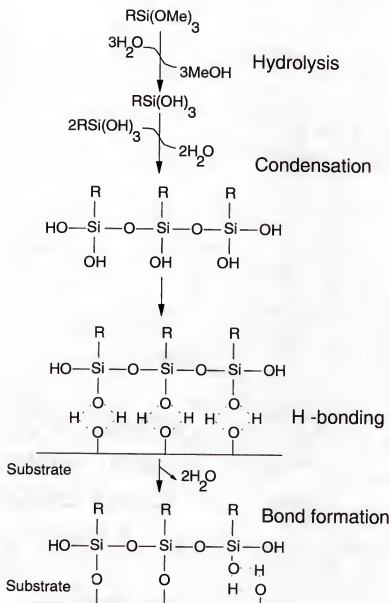


Figure 6-1 Deposition mechanism of silanes from aqueous media [Ark77].

product was then washed with water and dried under vacuum. This particular surface coating has been reported to have a zeta potential independent of both pH (over the range of 2-10) and length of the N,N-dimethyl-(m)-alkylamine used in the final reaction ( $m = 4$



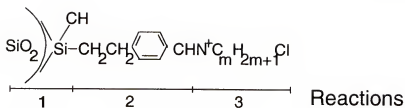


Figure 6-2 Diagram of the proposed final product of the three step silane reaction reported to have a pH independent surface charge. The subscript (m) represents the variable number of carbons which can be chosen for the alkyl used within the last reaction [Suh95].

to 8 carbons) [Suh95]. Such a coating would significantly help to simplify studies of the often interdependent charge and hydrophobicity variables.

#### 6-2-2 Surface Characterization

Streaming potential was used to monitor the apparent surface charge of the silanated glass slides (Fisher) and silanated engineering grade 200 micron diameter glass beads (Cataphote, Inc., Jackson MS) use within these studies. Streaming potential analysis on the glass beads were then conducted with the use of the device outlined in Chapter 2, while the glass slides were evaluated with the use of a flat plate streaming potential from a Van Wagenen and Andrade design [VanW80, Bat98]. Surface coated materials were placed within the streaming potential sample cells and initially rinsed with distilled water (pH 6.3) for one hour at approximately 1 liter/min. Streaming potential measurements were then carried out with a 0.1 mM KCl solution to monitor the zeta potential of the various surfaces. The samples were then flushed with multiple liters of distilled water at 1 liter/min and periodically monitored with the streaming potential to determine charge stability. Flow direction of the water used in the flushing procedure

was periodically reversed in order to ensure that dissimilar electrode environments did not develop in the proximity of the electrodes within the sample cell and produce false readings. The zeta potentials of the colloidal silica particles used within this study were determined with the use of a Brookhaven ZetaPlus electrophoresis instrument, model v3.21. Fourier Transform Infrared spectroscopy (FTIR) and Ultra Violet Visible spectroscopy (UV) were also used to monitor silane stability to water exposure. Tapping mode AFM was used to evaluate the coating uniformity and roughness of a silanized glass surface.

3DOT-EWLS was used in the final characterization of these coated surfaces. Colloidal silica particles, 1.5 micron diameter, were suspended in 0.1 mM or 0.4 mM KCl solution in a concentration between 1000 to 10000 particles/ml at a 6.3 pH. One of these particles was then captured within the optical trap and used to probe the silanated surface. Forty microliters of 10 micron spacer beads (Polysciences) were also added to the 10 ml silica suspension to prevent the collapse of the gap between the microscope slide and the cover slip. The edges of the cover slip were then sealed with silicon stopcock grease to prevent evaporation during analysis.

### 6-3 Results and Discussion

Coating stability under water flow was monitored to aid in the preliminary evaluation of the surface modifications proposed for use within the 3DOT-EWLS apparatus. The initial zeta potential of the N,N-DMBA chemically coupled coating appeared to have an initial zeta around +50 mV similar to values reported in the literature documenting the reaction procedure [Suh95]. After exposure to water, this charge fell

dramatically to negative zeta values implying a loss of the positive nitrogen species (Figure 6-3). FTIR results also confirmed this apparent loss of nitrogen from the glass surface. Further characterization of the silane elutriate with UV spectroscopy showed the presence of a benzene ring and suggested the loss of the chloromethylstyrene spacer used in the second step of the Suhara reaction. Attempts to monitor the instability of the TMCTS layer as a function of elution volume with the streaming potential device were complicated by the fact that the zeta potentials of the TMCTS coating glass were similar to those of the unmodified glass (Figure 6-4). The complicated chemical structure of the TMCTS (Figure 6-5) did not, however, appear to be capable of the covalent bonding mechanisms of Figure 6-1, which eventually led to the determination that the TMCTS was only surface polymerizing over the glass substrates [Meh97].

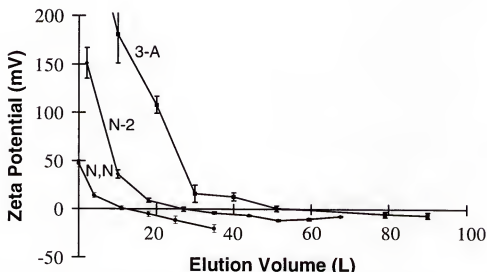


Figure 6-3 Graph showing streaming potential results as a function of water elution volume. Elution and streaming potential runs were performed at pH 6.3. Curves from right to left correspond to 3-APTES, N-2-AE-3-APTMS and the coupled N,N-DMBA.

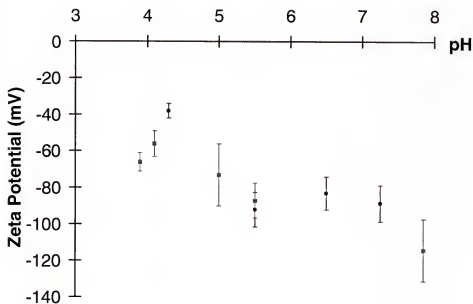


Figure 6-4 Zeta potential as a function of pH comparing acid washed glass beads before (round points) and after coating with TMCTS (square points).

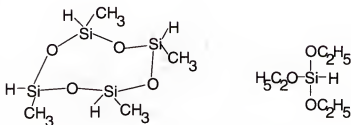


Figure 6-5 Structure of TMCTS as compared to triethoxysilane.

In an attempt to covalently bond the first step of this three step reaction to the glass, triethoxysilane was used in place of the TMCTS. The comparison of zeta potentials as a function of elution volume has been included as Figure 6-6 for both completed reactions. The modified Suhara reaction did appear to have a more stable positive surface charge. It is unclear however, as to whether the unique coating properties reported within the

literature for the three step reaction including TMCTS still hold true after triethoxysilane substitution. In addition, the multilayered deposition of the triethoxysilane from aqueous solution [Ark77, Moo97] still leaves questions as to the long term stability of this coating and the overall coating uniformity after water exposure (Figure 6-7).

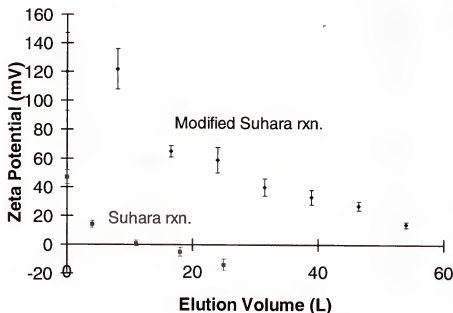


Figure 6-6 Comparison of the zeta potential of the N,N-DMBA coating as a function of elution volume and initial silanization reaction used. The Suhara reaction reflects the use of TMCTS and while the modified reaction reflects the use of triethoxysilane.



Figure 6-7 Possible multistep silanization reaction. The initial silanization occurs in multilayers in which a fraction of the silane condensation chains covalently bond to the glass. The remaining fraction of the multilayer will be physisorbed onto the covalently bound silanes. These outermost physisorbed silanes are the most probable sites for chemical functionalization and will not be covalently bound to the glass.

To avoid complications stemming from multiple reaction steps, simpler one step deposition reactions from aqueous solution were investigated. 3-Aminopropyl-triethoxysilane (3-APTES) and N-(2-Aminoethyl)-3-Aminopropyl-trimethoxysilane (N-2-AE-3-APTMS) coatings were deposited and evaluated for uniformity, stability and charge. Streaming potential results again indicated a rapid loss of positive coating character (attributed to the silane's amine groups) during elution to negative zeta values around  $-7 \text{ mV} \pm 3 \text{ mV}$  (Figure 6-3). This apparent loss of the silane coating due to water exposure has been well documented within the literature for all silanes including aminosilanes which are reported to be the most stable to hydrolytic breakdown [Goo90, Plu82, Che98]. AFM analysis (tapping mode) of the 3-APTES modified surface after water exposure indicated a relatively uniform coating (Figure 6-8). The overall root mean square (rms) of the roughness on the coated surface was determined to be 0.58 nm

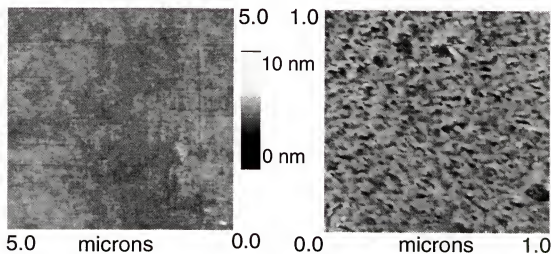


Figure 6-8 AFM tapping mode results showing surface topology of an unmodified glass slide (right) and a 3-APTES coated glass slide (left). Comparison of  $Z_{\max}$  (highest and lowest points) values showed the coated surface to be 1.7 nm larger than observed for the unmodified glass confirming the presence of a silane multilayer.

with a  $Z_{\text{max}}$  of 4.7 nm. The uncoated glass surface had a rms value of 0.28 with a  $Z_{\text{max}}$  of 3 nm. Values well below those reported for other “flat” surfaces being studied with modified AFM cantilevers (rms 3 nm) [Lar93]. Surface non-uniformities have been reported as one of the reasons behind disagreements between experimental observations and theory [Chapter 4, Eli95, Rya96, Hol97, Kap96]. The presence of heterogeneities in charge or roughness may significantly effect the reproducibility of force measurements as a function of slide position. AFM mapping of a washed 3-APTES modified glass slide, however, appeared to show a relatively uniform surface with no large masses of coating present.

The 3DOT-EWLS was used as both a qualitative and quantitative tool in evaluating the surface forces between colloidal glass particles and a 3-APTES modified surface (after 55 L of water exposure). The behavior of the colloidal silica particles interacting with the glass/modified glass surfaces have been documented within Table 6-1. The corresponding force and energy curves measured with the 3DOT-EWLS technique have been included as Figure 6-9.

Table 6-1 Qualitative and quantitative observations as made with 3DOT-EWLS for a silane modified and unmodified glass slide at pH 6.3

	KCl Concentration	Surface Zeta Potential	Colloidal Adhesion	Colloidal Brownian Motion	3DOT-EWLS
Unmodified Glass	$4 \times 10^{-4}$ M	-35 mV $\pm 3$ mV	Adhesion observed	Varying	[Cla99]
	$1 \times 10^{-4}$ M	-44 mV $\pm 3$ mV	No particle adhesion	Full	Fig. 6-10
3-APTES Glass	$4 \times 10^{-4}$ M	-5 mV $\pm 3$ mV	All very weakly adhered	Substantial (tethered)	Fig. 6-9
	$1 \times 10^{-4}$ M	-7 mV $\pm 3$ mV	No particle adhesion	Full	Fig. 6-9
Colloidal Silica Particle	$4 \times 10^{-4}$ M	-36 mV $\pm 3$ mV	NA	NA	NA
	$1 \times 10^{-4}$ M	-42 mV $\pm 3$ mV	NA	NA	NA

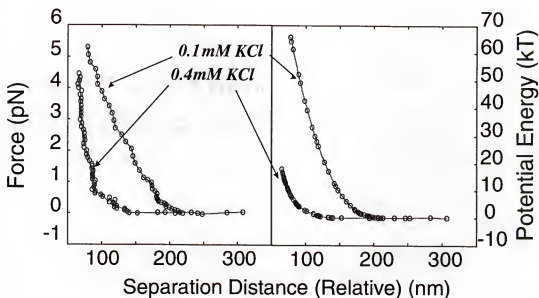


Figure 6-9 3DOT-EWLS force and energy curves for colloidal silica and 3-APTES modified glass at pH 6.3. Absolute spacing of total separation distances between the particle and the modified microscope slide were approximated with DLVO theory.



#### 6-4 Conclusion

3DOT-EWLS appeared to successfully measure forces between the colloidal glass particle and the silanated glass surface within an aqueous environment. The technique has in the past successfully measured surface forces for both biological and non-biological colloidal particles of small dimension (0.5 to 5 microns in diameter) with exceptional sensitivity (0.01 to 50 pN). The technique in these cases however, were limited to optically transparent unmodified glass surfaces. In this study, silanes were used to coat glass surfaces for 3DOT-EWLS analysis to determine their potential in producing a wide range of uniform van der Waals, double layer repulsion and hydrophobic interactions. It is however, important that these surface modifications meet several criteria for successful use within the 3DOT-EWLS device: Coating thickness must be kept at a minimum to ensure sufficient penetration of the evanescent wave into the surrounding aqueous media to allow for force measurements; the coatings must also be stable in aqueous environments and uniformly applied to the glass substrate to prevent dramatic variations in surface properties or trapping potential.

Comparisons between the 3DOT-EWLS data for the silanated glass/colloidal silica interaction (Figure 6-10) again showed a longer decay length in the energy-distance curve than predicted by DLVO theory. The exponential section of the glass-colloidal silica curve did agree fairly well with theory. A fact which appears to be in contrast to the force curves recorded for the modified 3-APTES glass surface. This discrepancy again suggests the possible importance of polymerized surface layer and its conformational behavior as a function of interaction force.

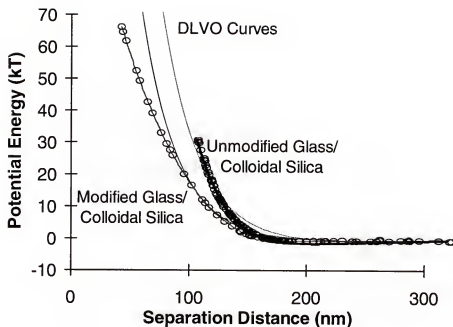


Figure 6-10 Comparison of 3DOT-EWLS data for unmodified glass and 3-APTES (after rinsing) coated glass surfaces interacting with colloidal silica for 0.1 mM KCl. Curves have been spaced at absolute separation distances with DLVO theory. The DLVO curves (solid lines) have been based on charge values included in Table 6-1 and a Hamaker constant for silica ( $6.6 \times 10^{-21}$  J).

#### 6-5 Summation

The surface silanization procedures used to modify interaction forces between 3DOT-EWLS surfaces showed considerable promise. Several of the silane modifications were stable enough after preliminary water elution for controlled interparticle studies (3DOT-EWLS measurement time with replication is on the order of hours). Control of surface uniformity and roughness will be of an additional importance to any glass modification prior to force analysis. Care must be taken to ensure that the measured energy curves are the result of specific surface properties being investigated and not a result of surface roughness or incomplete coverage. Future work should consider the use

of water plasma treatment prior to silanization to minimize overall surface roughness. Such treatment has been reported to reduce silane coating roughness to rms values on the order of 0.30 nm as opposed to the 0.58 nm values generally observed without plasma treatment [Alc99]. The use of silanes to vary surface charge, hydrophobicity, ligand concentration, chemical nature and potentially surface roughness will expand the overall usefulness of the 3DOT-EWLS technique in studying surface forces.

## CHAPTER 7 CONCLUSIONS AND FUTURE WORK

### 7-1 Colloidal Particles Under 3DOT-EWLS Analysis

The application of the 3DOT-EWLS technique in measuring the first ever interparticle forces between a glass surface and a spherical *S. aureus* microbe has been successful. The observed deviations between the 3DOT-EWLS measurements and DLVO theory still, however, remain unclear. A possible compression of the bacterial cell wall surface appendages was offered as a possible explanation to account for the deviation. Future work needs to be directed towards understanding the time scale over which the bacterial surface appendages (and even the silane polymers) compress or undergo conformational changes specifically in response to the 3DOT-EWLS measurement. The measurement itself allows for equilibration between the interaction forces and the particle within the optical trap. The measurement of the entire interaction curve takes several minutes and the forces acting upon the trapped particle accumulate with every incremental step towards the surface. The particle within the optical trap has the opportunity to respond to these forces over this several minute time scale resulting in some degree of equilibration between the surface forces and the surface polymers. These interactions of forces over several minutes may not be representative of the quick, non-equilibrium interactions expected for an interacting Brownian particle under natural conditions. To avoid equilibration complications from this gradual build-up of

interaction forces, the 3DOT-EWLS technique must measure every point on the force curve independently. In other words, instead of gradually approaching the surface in 10 nm steps, the force measurements must be compiled from a series of single measurements in which the particle is stepped towards the surface from a fixed reference position some large distance away. After this single measurement, the particle would then be returned to the fixed position and again stepped toward the surface to a different point of separation. The fixed reference position would be 200-300 nm away from the glass surface in order to prevent any type of particle interactions before each force measurement. This type of single measurement approach could then be applied multiple times to produce curves such as those shown in Chapters 5 and 6. Such measurements could provide important information as to the conformation and structural properties of various surface polymers.

The effectiveness of the 3DOT-EWLS technique in measuring interparticle forces for non-spherical microorganisms is also still unclear. Spherical particle geometries are assumed within the 3DOT-EWLS calculations of interparticle force. In addition, surface inhomogeneities or deviations from the spherical geometry will lead to a preferential orientation of the particle/microbe within the optical trap. Force measurements on these types of systems may not adequately represent the other non-interacting particle surfaces. Periodic reorientation of non-spherical or semi-spherical particles within the trap would also lead to a larger variance within the particle scatter signal. Preliminary measurements on the gram positive *Streptococcus fecalis*, a less perfectly spherical microbe than the

*S. aureus*, have suggested this particular type of increased variance within the particle scatter. Use of the 3DOT-EWLS technique in the development of a comprehensive understanding of microbial deposition must be based upon a wider sampling of bacteria.

3DOT-EWLS technique could also be an effective tool in studying the effects of chemical and genetic modifications to the bacterial surface. The *S. aureus* cell wall can be modified through mutation or through chemi and physisorption of surface active species. Comparisons between various *S. aureus* mutant strains could provide significant insight as to the importance of specific membrane proteins in regulating bacterial surface charge. Surface active agents as chitsan, known for its adsorption and modification of membrane properties, could also be thoroughly studied. In addition, bacterial ligand properties could be investigated by genetically varying bacterial receptor length and surface densities in conjunction with protein (ligand) modified glass surfaces by chemically coupling various proteins to the 3DOT-EWLS glass surface via the silane reactions of Chapter 6.

### 7-2 Substrates under 3DOT-EWLS analysis

The generation of an evanescent wave is a key part in the determination of particle interaction forces by the 3DOT-EWLS device. To this end, certain limitations must apply to the selection and type of surfaces studied. The use of glass dovetailed prisms and slides are the most cost effective choice for this task. This decision, however, significantly limits the variety and types of forces probed by the colloidal particle. Silane modifications provide an attractive means of modifying the glass surface properties. The importance of careful characterization of these silanated surfaces must again be

reemphasized. Silane stability in aqueous media is tenuous and many of the modified glass surface properties appear to change as a function of time when exposed to water. These silanated glass surfaces should be used only after the weakly bonded physisorbed silanes precipitates have been removed from the surface as suggested by the streaming potential studies of Chapter 6. Otherwise, surface properties such as charge, hydrophobicity and surface roughness may vary during the course of the experimental run.

### 7-3 Investigation of Oil Emulsion Interactions with Solid Surfaces

Initial 3DOT-EWLS measurements on an oil in water emulsion at high surfactant concentrations also appeared to be encouraging (anionic surfactant sodium dodecyl sulfate (SDS), hexadecane (refractive index 1.423) and water in a 3:6:91 (w/w/w) ratio). The anionic surfactant was used to increase the overall repulsion of the hexadecane droplet with the glass surface. This was done in order to stabilize the oil droplet and prevent irretrievable migration of the droplet to the glass due to its inherent buoyancy within the aqueous continuous phase. Recall that the 3DOT-EWLS microscopic technique requires samples to be placed within an inverted microscopy system. Figure 7-1 has been included showing one such measurement between the hexadecane/surfactant colloidal emulsion drop and the glass surface. The DLVO curve fit represents an assumed charge value corresponding to a geometric mean of -15 mV and a Hamaker constant of  $2.5 \times 10^{-20}$  J (a value larger than predicted via theory,  $7 \times 10^{-21}$  J, which may reflect the presence of a buoyancy force). In addition, the Debye length used within the DLVO calculation was substantially larger than otherwise predicted from

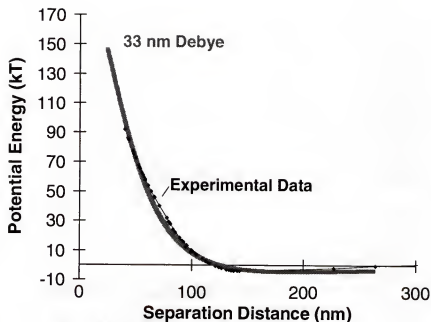


Figure 7-1 3DOT-EWLS data (diamond points) for an emulsion droplet (SDS, hexadecane and water 3:6:91 w/w/w ratio). A DLVO curve (solid line) was fit to the data.

solution conditions. A Debye length of 30 nm which corresponded to an ionic strength of 0.1 mM was required to fit the experimental data. A value much larger than expected for the weight percent of surfactant used within this system. Again, the effect of the buoyancy within the system may in fact place a significant role in force measurements and may act as a restoring force against the droplet displacement within the optical trap. Additional concerns about droplet deformation also need to be addressed before any in-depth 3DOT-EWLS experimentation.



## APPENDIX A STREAMING POTENTIAL DESIGN

The streaming potential apparatus was constructed from readily available materials. The sample cell was created from a piece of clear polycarbonate pipe in order to allow for visual inspection and verification as to the absence of air pockets and overall packing uniformity between the electrodes. The inner diameter (I.D.) for this sample cell was chosen to be 1.9 cm (0.75 inches) to minimize possible wall effects for granular media with a diameter equal to or less than 1.5 mm (I.D.  $\gg$  diameter of sand). The length component of the sample cell was another important design consideration necessary to ensure reproducible measurements for granular media. Smaller sample cells where the packed bed length was less than 20 cm (8 inches) produced erratic zeta potential readings for materials with particle diameters greater than 0.7 mm (Figure A-1(A)). This inconsistent behavior was attributed to pressure fluctuations within the granular sample bed during operation.

The removable portion of the sample cell, Figure A-1(B), supported the electrode and allowed for some adjustment of the volume within the sample cell to ensure similar environments for both electrodes with no voidages or gas pockets within the granular media [Hor78]. The electrodes themselves consisted of 99% pure 18 gauge silver wire and 40 mesh sized silver gauze (Newark Wire Cloth Co., Newark, NJ). These components were spot welded together so that the silver wire could extended

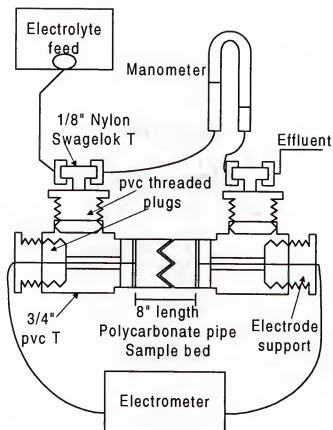


Figure A-1(A). Diagram of the simple streaming potential system used to approximate the surface potential of granular media.

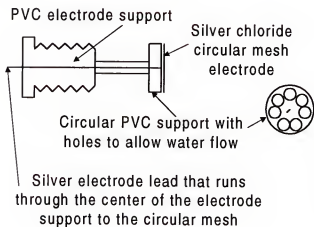


Figure A-1(B). Diagram of the inner electrode support used at both ends of the cylindrical packed bed shown above.

perpendicular from the center of the circular mesh. The mesh portion of the resulting union was then anodized with 5 milliamps (Bio Rad, power pac model 300) in a 0.1 N hydrochloric acid solution with a copper cathode for 1 hour in order to chloridize the silver [Jan61]. The finished electrodes had a brown to grayish plum color and were allowed to age overnight in  $10^{-4}$  M KCl solution. The electrodes were then sealed into the electrode supports as shown in Figure A-1(B). It has been strongly suggested that these electrodes be regenerated or replaced every three weeks to ensure proper performance. The semi-harsh environment around the electrodes, particularly during sample loading, may wear down the coating. In the absence or degradation of the silver chloride, the electrodes will no longer process the generated voltage signal produced within the apparatus in a phenomena commonly known as electrode polarization.

Before actual use of the streaming potential apparatus, three operational factors should be considered: 1) The evaluation procedure requires 60 milliliters of packed bed material; 2) Temperature must be consistently maintained or the temperature dependence of  $\mu$  and  $\epsilon$  must be accounted for in equation (2.2); 3) Care must be taken if and when conductive materials are used in the construction of this device such as unions, pumps or pressure transducers. The use of conductive materials will result in some degree of electrical interference and a dramatic decrease in the signal to background noise ratio. Ultra high impedance differential amplifiers and/or a Faraday cage can be used to reduce the noise problem if such alterations are desired [van80].

The overall setup of this device required an electrometer (Keithley Instruments 610C) to be connected to the silver chloride electrodes to measure voltage drop and a water manometer to monitor the pressure drop of the flowing electrolyte. The remaining

tubing ports were used to purge the packed bed with CO<sub>2</sub> before analysis to lessen the risk of air pockets within the sample media and allow for the gravity feed of weak KCl electrolyte solution (Figure A-1(A)).

Preparation of the sample prior to analysis required the granular media to be systematically rinsed in a nylon mesh sieve tray with distilled water. This was done to remove loose particulate material from the granular surfaces which could result in dissimilar environments of the upstream and downstream electrodes during operation. After packing the media into the sample cell, one to two liters of KCl solution were generally allowed to flow through the packed bed (1 liter/hr) to further rinse and equilibrate the sample. All experimental runs were performed with the use of 10<sup>-4</sup> M KCl solution under laminar flow conditions. During the actual measurement procedure the electrodes were used to monitor the electromotive force generated as the charged ions in the electrolyte solution passed the charged sample surface under investigation. These voltage measurements were performed as a function of the pressure drop across the sample bed. After recording a voltage and pressure reading the electrolyte flow was stopped and the electrometer was allowed to return to its zero potential. The voltage measurement was then corrected to account for any deviation away from the zero. This procedure was followed for multiple voltage and pressure drops in order to collect enough data to plot voltage versus pressure drop (Figure A-2). The slope from the measured voltage and pressure drop data along with solution conductivity were then used to calculate the corresponding zeta potential ( $\zeta$ ) via the Smoluchowski relation (2.2). The plot of the resulting voltage/pressure drop line in general will not pass through the origin

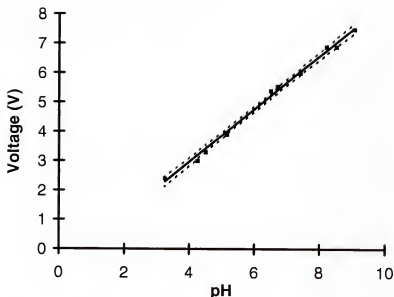


Figure A-2. Sample data from the streaming potential analysis of metal hydroxide coated Ottawa sand after 62 days of exposure to wastewater flow for conditions of pH 4.3. Linear regression was used to determine the slope and the corresponding 95% confidence band (dashed lines) shown here. The full pH curve for this biosystem has been shown as Fig. 2-10.

(Figure A-2 shows the intercept to be -0.64 mV). This "erratic rest potential" has been a common observation throughout the streaming potential literature [van80, Eag77, Bal73, Fit72]. This absence of a non-zero intercept has many times been mistaken to indicate poor quality results. Several of the above mentioned authors have noted however, that this time dependent deviation does not effect the slope of the voltage/pressure line used in the Smoluchowski equation and thus the calculated zeta potential. A thorough investigation by van der Put [van80] attributed these erratic rest potentials to salt rejection by the porous media sample. This in turn has resulted in the violation of the initial assumption that the  $\frac{d \ln C}{dx}$  term could be set to zero in the simplification of equation (2.1). Adequate results, however, can be obtained through equilibration procedures as

outlined above and careful monitoring of the influent and effluent electrolyte conductivity and pH. In the case of biofilms or unstable coatings where solution contact time may be an issue, analysis procedures may begin as soon as the conductivity and pH values for the electrolyte solution entering and leaving the sample cell are the same. The streaming potential measurements under these less equilibrated conditions will, however, exhibit greater erratic rest potentials and complications due to the drifting of the voltage readings as measured with the electrometer.

## APPENDIX B

### ORIGIN OF CHARGE WITHIN THE METAL HYDROXIDES

The differences in charge between the metal oxide and the metal hydroxide have recently been explained with the use of Pauling's bond valence principles and a concept of proton affinity [Hie96]. Briefly defined, proton affinity is a term used to describe the driving force an oxygen atom experiences in an attempt to neutralize its charge originating from the undersaturation of its valence electrons. The degree to which this proton affinity develops is in turn a function of two parameters. First, the overall number of metal and H ions coordinating to the oxygen. Secondly, the degree to which other atoms can be used to achieve electroneutrality of the oxygen within the metal (hydr)oxide. In terms of charge neutralization of the oxygen the overall charge can be thought of as being "distributed over the surrounding ligands, which can be expressed per bond" [Hie96]. The number of the allowable bonds to the metal cation and the oxygen is of course defined by the number of valence electrons present. So, if all of the possible bonds were filled and the electrons completely transferred to the receiving atom (in this case the oxygen), electroneutrality would be achieved. Complete transfer of these electrons does not occur however and the actual degree of transfer and the subsequent degree of charge neutralization will be a function of the position of the electrons within the bonds between the metal cations (Me) and the ligands (O or OH). The concept of Pauling's bond valence quantifies the fraction of donated charge that actually is available for use by the oxygen in the charge neutralization process. It is this final undersaturation

of the oxygen after all of the donated electrons have been considered, that results in the proton affinity of the metal hydroxides and the resulting positive character of the metal hydroxide relative to the metal oxide.

Equations describing the rate constant of the proton neutralization reaction can be expressed in terms of a proton affinity constant ( $K$ ),

$$\log K = -A[(S_{Me} + mS_H + n(1 - S_H))] + V \quad (\text{B.1})$$

where  $S_{Me}$  represents the bond valence of the metal ion (charge of the metal cation divided by the cations coordination number),  $S_H$  is the bond valence of the H donating bond,  $(1 - S_H)$  is the bond valence accepted by the oxygen through hydrogen bonding,  $V$  representing the valence of the oxygen within the mineral structure,  $A$  a constant of 19.8,  $m = \#$  of hydrogen bonds being donated and  $n = \#$  of hydrogen bonds being accepted. As the above equation shows, the number of hydrogen bonds being donated ( $m$ ) has a larger influence on increasing the intrinsic proton affinity constant ( $\log K$ ). An oxide complex in which the metal ion has three empty valence positions would result in  $n=3$  and  $m=0$ . While for a hydroxide the number of hydrogen bonds being donated and accepted would be,  $n=2$  and  $m=1$ . The resulting intrinsic proton affinity for the metal hydroxide would therefore be larger than for the metal oxide which translates into a higher pzc value and a larger pH range over which the surface charge will be positive.

Note that the above explanation is a somewhat idealized consideration of the origins of the charge in metal (hydr)oxide species and it should be realized that hydrogen bonding, Me-O bond distance and repulsion based lattice straining also effect the distribution of electrons within the bonds between the metal cation and the O and OH



groups. For a more in-depth discussion of the topics described both above and below please refer to Hiemstra, Venema and Van Riemsdijk [Hie96].

Gibbsite ( $\text{Al}(\text{OH})_3$ ), one of the mineral forms expected to be present within the precipitated coatings, is a mineral species with a simple well defined surface having only one type of reactive group which make this surface coating a relatively simple one to envision when considering the origin of charge. Gibbsite has a hexagonal structure with two types of crystal faces. These faces include a dominant 001 face and edge face parallel to the c-axis [Bra65]. The 001 face sites, however, have been shown not to be proton reactive in the pH range between 4 and 10 [Hie89]. This means that the edge faces of the gibbsite crystal are responsible for the material's charging through the protonation of the singly coordinated hydroxyl surface group:  $\text{AlOH}^{(6-1)} + \text{H}^+ \rightleftharpoons \text{AlOH}_2(\text{s})^+$ . The resulting proton affinity calculations predict a point of zero charge (pzc) around pH  $10 \pm 0.5$  [Hie96].

Goethite ( $\alpha$ - $\text{FeOOH}$ ) another of the expected mineral species has a more complex structure. The apparent main crystal plane of this mineral is the 110 face [Sch91] which is dominated by triply coordinated surface  $\text{Fe}_3\text{O}(\text{H})$  groups. The crystal structure of goethite can be described as  $\text{Fe}^{3+}$  ions hexagonally coordinated with O and OH groups (each O or OH coordinated with three  $\text{Fe}^{3+}$  ions). The bulk of the  $\text{FeOOH}$  contains two types of triply coordinated oxygen groups. One of which is protonated ( $\text{Fe}_3\text{OH}$ ) and the other group nonprotonated ( $\text{Fe}_3\text{O}$ ). The protonated group forms a hydrogen bond with the nonprotonated group. This asymmetric H bond leads to a  $\text{Fe}_3\text{OH-OFe}$  configuration [Hie96] where the resulting bond valence and bond lengths are distorted and give rise to

some of the goethite's proton affinity, the relatively high pzc ( $9.5 \pm 0.5$ ) and the corresponding positive surface character at pH values less than pzc. The dominant 110 crystal face consists of four different surface groups:  $\text{Fe}_1\text{O}_{\text{II}}$ ,  $\text{Fe}_2\text{O}_{\text{II}}$ ,  $\text{Fe}_3\text{O}_{\text{I}}$  and  $\text{Fe}_3\text{O}_{\text{II}}$ . Where the  $\text{Fe}_3\text{O}_{\text{II}}$  is the only species expected to negligibly contribute to the protonation constant.

Silica or the  $\text{SiO}_2$  surface is quite different in comparison to the metal (hydr)oxides. When comparing the pzc of these three surface one must realize that in the case of silica all the surface active groups are protonated and result in the uncharged  $\text{SiOH}^0$ . The metal hydroxides on the other hand are only fractionally protonated at their respective pzc values [Hie96]. This translates into the situation where the pzc of the silica occurs at much lower pH values (2.0) and results in the negative surface character above the pzc.

## APPENDIX C

### “OPTIMAL” PERFORMANCE

In order to produce an efficient and cost effective alternative to ordinary sand filtration it is important to define what is meant by developing and “optimal” surface for particle removal. As previously mentioned, the role of electrostatic interactions in particle deposition can be viewed in terms of DLVO theory [Ver48, Der41]. Figure 1-1 illustrated two regions of particle deposition predicted by DLVO theory for the interaction between two charged surfaces of varying sign and magnitude. The energy barrier limiting regime where particle deposition would not occur and the transport limited regime where particle deposition is controlled by particle convection and diffusion. Since the convective and diffusive properties were not manipulated within these studies, the transport regime would correspond to “optimal” particle removal conditions in the simplest sense. The theory suggests that an optimally coated system would correspond to a surface charge roughly equivalent to -0.5 mV for most bacterial systems. The tool by which the collector surface charge is approximated is however a macroscopic tool and measures zeta potential as if all charges were homogeneously distributed over the collector’s surface. On the microscopic scale, the surface is covered with favorable particle interaction sites that are transport limited as well as unfavorable particle interaction sites with energy barrier requirements. This is still the case for a heterogeneously charged surface with an overall net negative zeta potential. The

deposition would in these cases be due to the statistical probability that an effluent particle would be in the right place on the collector's surface to experience favorable particle interactions, a transport-driven interaction. This would mean that an "optimal" surface coating would require only a certain number of these favorable microscopic sites on the collector media. That certain number would reflect the surface area of the collector, the length of the packed bed, as well as, the convective and diffusive properties of the microbes in order to ensure that the microbes entering the filter would have a very high probability of being captured. In this sense, without considering any steady state biofilm growth on the collector's surface, an "optimal" media would exist even with a net negative zeta potential. The determination of the exact value of this negative charge would be quite difficult but for purposes of estimating cost, a value of -40 mV has been assumed. From the commercial perspective however, quality assurance on five tons of these filter materials would require an easier benchmark of the zeta potential such as our initial -0 mV standard. This parameter could be relatively easily measured for any such surface modification process if such a coating process was ever deemed feasible.

The decision to modify ordinary filtration sand was one based on economics. Other positively charged aluminum oxide granules or metal containing ores are readily available for usage in 5 ton sand filters. The cost of these materials are obviously much higher than expected for plain sand. A cost comparison between an aluminum oxide granular media and the proposed metal (hydr)oxide coated media was performed to determine the cost effective nature of the proposed coating procedure. Table C-1 has been included below with a net present worth evaluation between a five ton filter filled with aluminum oxide as well as a standard and "optimized" metal precipitate coating with

12% depreciation. The amounts of metal precipitate present on the granular surfaces corresponding to the standard deposition state (before coating loss) and an “optimum” state (zeta potential -40 mV) were determined with the use of Induced Coupled Plasma spectroscopy. A five year lifetime was assumed for the aluminum oxide coating, a conservative estimate based on the lifetime of silica within a standard packed bed filtration system. A lifetime for the precipitated coating materials was then assumed to be 4 months to allow for a comparison. The Table C-1 analysis suggested that modification of silica surfaces to promote particle deposition is not truly cost effective for a four month coating lifetime. At present, the coating lifetime corresponding to optimal removal conditions appears to be merely on the order of several days in an open loop stationary bed filtration system (see Figure 2-9). This coating instability combined with past speculation linking certain forms of aluminum in drinking water to Alzheimer’s disease [Del88] makes this proposed filtration application commercially unattractive.

Table C-1 Cost analysis of proposed metal (hydr)oxide coatings

Table 3-2	Aluminum Oxide	Standard Coating	Optimal Coating
Initial Investment	\$3,500.00	\$766.00	\$711.00
Year 1		\$853.00	\$706.00
Year 2		\$1,016.00	\$840.00
Year 3		\$907.00	\$750.00
Year 4		\$810.00	\$670.00
Year 5		\$723.00	\$599.00
Net Present Worth	\$3,500.00	\$5,076 +equipment	\$3,570 +equipment

## REFERENCES

- Abb83    Abbott A. Rutter P.R. Berkeley R.C. J. Gen Microbiol. 129 (Pt 2) 439-445 (1983).
- Ach94    Achouak W. F. Thomas F. and Heulin T. Colloids and Surf. B: Biointerfaces 33 131-137 (1994).
- Act88    "Antibiotic Inhibition of Bacterial Cell Surface Assembly and Function". Actor, P. ed. Washington, D.C.: American Society of Microbiology (1988).
- Ada95    Adair J. Unpublished data from the Department of Materials Engineering, University of Florida (1995).
- Ada76    Adamson A. W. "Physical Chemistry of Surfaces." New York: Wiley (1967).
- Ait81    Ait'ian S. Belaia M.L. and Chizmadzhev I. Biofizika. 26 (4) 701-708 (1981).
- Ake90    Akesson T. Woodward C. and Jonsson B. Progress in Colloid & Polymer Science 81 268 (1990).
- Alc99    Alcantar N.A. Aydil E.S. and Israelachvili J.N. Proceedings of the 7th International Symposium on Chemically Modified Surfaces. Little C.B. and Blitz J.P. eds. Cambridge, UK: Royal Society of Chemistry (1999).
- Ark77    Arkles B. Chemtech 7 766-778 (1977).
- Ash86    Ashkenazi S. Weiss E. and Drucker M.M. J. Lab. Clin. Med. 107 (2) 136-140 (1986).
- Ash92    Ashkin A. Biophys. J. 61 569 (1992).
- Bal73    Ball B. and Fuerstenau D.W. Miner. Sci. Eng. 5 267-277 (1973).
- Bal88    Baloda S.B. Faris A. and Krovacek K. Microbiol. Immunol. 32 (5) 447-459 (1988).
- Bae76    Baes C.F. and Mesmer R.E. "Hydrolysis of Cations." New York: Wiley (1976).

- Bas88 Bashan Y. and Levanony H. J. Ge. Microbiol. 134 2269-2279 (1988).
- Bat98 Batich C. Unpublished data from the Department of Materials Engineering, University of Florida (1998).
- Ben80 Ben-Naim A. "Hydrophobic Interactions." New York: Plenum Press (1980).
- Ber80 Berkeley R.C.W. "Microbial Adhesion to Surfaces." New York: Halsted Press (1980).
- Bir60 Bird R.B. Stewart W.E and Lightfoot E.N. "Transport Phenomena." New York: Wiley (1960).
- Bow79 Bowen B.D. and Epstein M.J. J. Colloid and Interface Sci. 72 81-97 (1979).
- Bow98 Bowen W.R. Hilal N. Lovitt R.W. and Wright C.J. Colloids and Surf. A 136 231-234 (1998).
- Bra65 Bragg L. and Claringbull G.F. in "The Crystalline State." L. Bragg ed. Vol. IV London: Bell and Sons (1965).
- Bri65 Brinton C.C. Jr. Trans N Y Acad. Sci. 27 (8) 1003-1054 (1965).
- Cla99 Clapp A. Ruta A. and Dickinson R. Submitted for review Rev. Sci. Instrum. (1999).
- Che98 Chen J. Truesdail S. Lu F. Zhan G. Belvin C. Koopman B. Farrah S. and Shah D. J. Water Res. 32 (7) 2171-2179 (1998).
- Che79 Chew H. Wang D.S. and Kerker M. Applied Optics 18 2679 (1979).
- Cra97 Craig V.S.J. Colloids and Surf. A: 129-130 75-94 (1997).
- Del88 Delves H.T. Suchak B. and Fellows C.S. "Aluminum in Food and the Environment." Proceedings of a Symposium, Environment and Food Chemistry Groups R. Massey and D. Taylor eds. London: Royal Society of London 52 (1988).
- Der41 Derjaguin B. and Landau L. Acta Physicochim 14 733-762 (1941).
- Der64 Derjaguin B.V. Voropayeva T.N. Kabanov B.N. and Titiyevskaya A.S. J. Colloid Interface Sci. 19 113 (1964).
- Dic97 Dickinson R.B. J. Colloid Interface Sci. 190 142-151 (1997).

- Don91 Donaldson S.G. Azizi S.Q. and Dal Nogare A.R. Am. Rev. Respir. Dis. **144** (1) 202-207 (1991).
- Dru89 Drumm B. Neumann A.W. Policova Z. and Sherman P.M. J. Clin. Invest. **84** (5) 1588-1594 (1989).
- Duc91 Ducker W.A. Senden T.J. and Pashley R.M. Nature **353** 239 (1991).
- Duc92 Ducker W.A. Senden T.J. and Pashley R.M. Langmuir **8** (7) 1831-1836 (1991).
- Duk74 Dukhin S.S. and Derjaguin B.V. "Surfaces and Colloid Science." Matijevic E. ed. New York: Wiley 7 (1974).
- Dyo96 Dyomin V.V. and Sokolov V.V. "Holographic diagnostics of biological microparticles." Proceedings of SPIE - The International Society for Optical Engineering **2678** 534-542 (1996).
- Eag77 Eagland D. and Allen A.P. J. Colloid Interface Sci. **58** 230 (1977).
- Ego94 Egorova E.M. Electrophoresis **15** (8-9) 1125-1131 (1994).
- Eli90 Elimelech M. O'Melia C.R. Langmuir **6** 1153-1163 (1990).
- Eli95 Elimelech M. Gregory J. Jia X. and Williams R.A. "Particle Deposition and Aggregation: Measurement, Modeling and Simulation." Oxford: Butterworth-Heinemann Ltd. (1995).
- Els97 El-Shall H. Unpublished data from Global Consulting Co. Gainesville, FL (1997).
- Fai91 Fairhurst D. and Ribitsch V. "Particle Size Distribution II, ACS Symposium." Series No. 472 Provder T. ed. Washington, D.C.: American Chemical Society 337-353 (1991).
- Fit72 Fitzpatrick J.A. "Mechanisms of Particle Capture in Water Filtration." Ph.D. Thesis Cambridge, MA: Harvard University (1972).
- Fix83 Fixman M.J. Chem. Phys. **78** 1483 (1983).
- Fra97 Frank B.P. and Belfort G. Langmuir **13** 6234-6240.
- Fre79 Freeman A.B. "Burrows Textbook of Microbiology." 21st ed. Philadelphia: Saunders (1979).



- Gal87 Galdiero F. Cotrufo M. Catalanotti P.G. De Luca T.S. Ianniello R. and Galdiero E. Eur. J. Epidemiol. **3** (3) 216-221 (1987).
- Ger81 Gerba C. Goyal S.M. Cech I. and Bogdan G.F. Environ. Sci. Technol. **15** 940-944 (1981).
- Gie98 Giesbrecht P. Kersten T. Maidhof H. and Wecke J. Micro. Molec. Biol. Rev **62** (4) 1371-1414 (1998).
- Gil91 Gilbert P. Evans D.J. Evans E. Duguid I.G. and Brown M.R. J. Appl. Bacteriol. **71** (1) 72-77 (1991).
- Gil95 Gilson M.K. Curr. Opin. Struct. Biol. **5** (2) 216-223 (1995).
- Goo90 Goodwin J.W. Harbron R.J. and Reynolds P.A. Colloid Polym. Sci. **268** (8) 766-777 (1990).
- Gra93 Grabbe A. and Horn R.G. J. Colloid Interface Sci. **157** 375-383 (1993).
- Gre80 Gregory J. and Wishart A.J. J. Colloid Interface Sci. **1** 313-334 (1980).
- Hie87 Hiemstra T. De Wit J.C.M. and Van Riemsdijk W.H. J. Colloid Interface Sci. **133** 105 (1989).
- Hie96 Hiemstra T. Venema P. and Van Riemsdijk W.H. J. Colloid Interface Sci. **184** 680-692 (1996).
- Hie97 Hiemenz P.C. and Rajagopalan R. "Principles of Colloid and Surface Chemistry." New York: Marcel Dekker (1997).
- Hig97 Higashitani K. and Ishimura K. J. Chem. Eng. of Japan **30**(1) 52-58 (1997).
- Hog66 Hogg R. Healy T.W. and Fuerstenau D.W. Trans. Faraday Soc. **62** 1638-1651 (1966).
- Hol97 Holt W.J.C. and Chan D.Y.C. Langmuir **13** 1577-1586 (1997).
- Hon84 Honig B. Prog. Clin. Biol. Res. **164** 149-152 (1984).
- Hor78 Horn J.M. "Electrokinetic Properties of Silica, Alumina and Montmorillonite." Ph.D. Thesis Gainesville, FL: University of Florida (1978).
- Hsu94 Hsu J. and Kuo Y. J. Colloid and Interface Sci. **166** (1) 208-214 (1994).
- Hul69 Hull M. and Kitchener J.A. Trans. Faraday Soc. **65** 3093-3104 (1969).

- Isr78 Israelachvili J. and Adams G.E. J. Chem. Soc. Faraday Trans. I **74** 975 (1978).
- Isr92 Israelachvili J. "Intermolecular and Surface Forces." San Diego, CA: Academic Press (1992).
- Jac75 Jacobson K. and Papahadjopoulos D. Biochemistry **14** (1) 152-161 (1975).
- Kag99 Jaganathan A. "Direct Measurement of Polymer-Induced Forces." Ph.D. Thesis Gainesville, FL: University of Florida (1999).
- Jan61 Janz G.J. "Reference Electrodes, Theory and Practice." G.J. Janz and D.G. Ives eds. New York: Academic Press (1961).
- Joh96 Johnson P.R. Sun N. and Elimelech M. Environ. Sci. Technol. **30** 3284-3293 (1996).
- Jon97 Jonasz M. Applied Optics **36**(18) 4214 (1997).
- Jon83 Jones G.W. and Isaacson R.E. Crit. Rev. Microbiol. **10** 229-260 (1983).
- Juc96 Jucker B.A. Harms H. and Zehnder A.J. J. Bacteriol. **178**(18) 5472-5479 (1996).
- Juc98 Jucker B.A. Zehnder A.J.B. and Harms H. Environ. Sci. Technol. **32** 2909-2915 (1998).
- Kap96 Kapur R. Lilien J. Picciolo G.L. and Black J. Bio. Mat. Res. **32** (1) 133-142 (1996).
- Kar97 Karaman M.E. Pashley R.M. Waite T.D. Hatch S.J. and Bustamante H. Colloids and Surf. A: **129-130** 239-255 (1997).
- Kin93a Kinoshita T. Bales R.C. Yahya M. and Gerba C.P. Wat. Res. **14** (8) 1295-1301 (1993).
- Kin93b Kinoshita T. Bales R.C. Yahya M. and Gerba C.P. Contaminant Hydrology **14** 55-70 (1993).
- Kle84 Klein J. and Luckham P.F. Coll. Surf. **10** 65-76 (1984).
- Kra97 Krarup H.G. Linhart R.V. and Adair J.H. OPAL© for Windows™ Graphical Display of Hydrolysis Systems Shareware University of Florida Materials Science and Engineering Department <http://zirconia.mse.ufl.edu/opal.htm> (1997).

- Kre89 Krekeler C. Ziehr H. and Klein J. Experientia, **45** (11-12) 1047-1055 (1989).
- Kuy98 Kuyucak S. Biophys. J. **74** (1) 22-36 (1998).
- Lar93 Larson I. Drummond C.J. Chan D.Y.C. and Grieser F.J. Am. Chem. Soc. **115** 11885-11890 (1993).
- Lec93 Leckband D. Chen Y. Israelachvili J. Wickman H.H. Fletcher M. and Zimmerman R. Biotech. and Bioeng. **42** 167-177 (1993).
- Li97 Li Y. and Park C.W. J. Colloid Interface Sci. **185** 49-56 (1997).
- Lit97 Little B.J. Wagner P.A. and Lewandowski Z. "Geomicrobiology : Interactions Between Microbes and Minerals." Jillian F. Banfield and Kenneth H. Nealson eds. Washington, D.C.: Mineralogical Society of America **123** 1997.
- Lit92 Litton G.M. and Olson T.M. Environ. Sci. Technol. **27** 185-193 (1992).
- Lof97 Löffler G. Schreiber H. Steinhauser O. J. Mol. Biol. **270** (3) 520-534 (1997).
- Luk97 Lukasik J. Farrah S.R. Truesdail S.E. Shah D.O. Kona **45** (1) 87-91 (1997).
- Mad97 Madigan M.T. Martinko J.M. and Parker J. "Biology of Microorganisms." Princeton, NJ: Prentice Hall (1997).
- Mar92 Marcelja S. Biophys. J. **61**(5) 1117-1121 (1992).
- Meh97 Mehta P. Huls America Personal Communication April 1997.
- Mit92 Mittal K. L. "Silanes and Other Coupling Agents." VSP (1992).
- Moo97 Moon J. H. Shin J. W. and Park J. W. "Molecular Crystals and Liquid Crystals Science and Technology, Section A: Molecular Crystals and Liquid Crystals." Proceedings of the 1996 1st Asian Symposium on Organized Molecular Films for Electronics and Photonics 294-295 Tsukuba, Japan: ASOMF'1 185-188 (1997).
- Mur80 Murray J.P. and Parks G.A. in "Particulates in Water." Adv. in Chem. Ser. **189** M.C. Kavanaugh and J.O. Leckie eds. Washington, D.C.: American Chemical Society 97-133 (1980).
- Mur97 Murray D. Ben-Tal N. Honig B. and McLaughlin S. Structure. **5** (8) 985-989 (1997).

- Nai93 Naito Y. Tohda H. Okuda K. and Takazoe I. Oral Microbiol. Immunol. **8** (4) 195-202 (1993).
- Nas97 Nassif X. Marceau M. Pujol C. Pron B. Beretti J.L. and Taha M.K. Gene **192** (1) 149-153 (1997).
- Nic93 Nicholov R. Khoury A.E. Bruce A.W. and DiCosmo F. Cells and Mater **3** (3) 321-326 (1993).
- Nre89 Nrekler C. Ziehr H. and Klein J. Experientia **45** 1047-1055 (1989).
- O'Br81 O'Brien R.W. and Hunter R.J. Can. J. Chem. **59** 1878 (1981).
- Ove52 Overbeek J. Th. G. "Electrokinetic Phenomena. Colloid Science." Vol. I H.R. Kruyt ed. Amsterdam: Elsevier Publishing (1952).
- Par65 Parks G. A. Chem. Rev. **65** 177 (1965).
- Pas85 Pashley R.M. McGuiggan P.M. Ninham B.W. and Evans D.F. Science **229** (4718) 1088-1089 (1985).
- Pea80 Pearce W.A. and Buchanan T.M. "Bacterial Adherence." E.H. Beachey ed. New York: Chapman and Hall Ch. 10 (1980).
- Pes76 Peschel G. and Belouschek P. Prog. Colloid Polym. Sci. **60** 108 (1976).
- Ple95 Plette A.C.C. Van Riemsdijk W.H. Benedetti M.F. and Van der Wal A. J. Colloid Interface Sci. **173** 354-363 (1995).
- Plu82 Plueddemann E.P. "Silane Coupling Agents." New York: Plenum (1982).
- Pop89 Popescu A.I. Gheorghe V. Physiologie **26** (4) 323-330 (1989).
- Pri76 Prieve D.C. and Ruckenstein E. J. theor. Biol. **56** 205-228 (1976).
- Pri87 Prieve D.C. Luo F. and Lanni F. Faraday Discuss. Chem. Soc. **83** 297 (1987).
- Ran84 Rand R.P. and Parsegian V.A. Can. J. Biochem. Cell Biol. **62** (8) 752-759 (1984).
- Ray36 Rayleigh J.W.S. Proceedings of the Royal Society of London Ser. A **156** 326 London: Royal Society of London (1936).
- Raz98 Razatos A. Ong Y.L. Sharma M.M and Georgiou G. J. Biomaterials Science-Polym. Ed. **9** (12) 1361-1373 (1998).

- Rob77 Robertson J.N. Vincent P. Ward M.E. J. Gen. Microbiol. 102 (1) 169-177 (1977).
- Rob98 Robertson S.R. and Bike S.G. Langmuir 14 928-934 (1998).
- Ron90 Ronner U. Husmark U. and Henriksson A. J. Appl Bacteriol. 69 (4) 550-556 (1990).
- Ros82 Rosenberg M. Bayer E.A. Delarea J. and Rosenberg E. Appl. Environ. Microbiol. 44 929-937 (1982).
- Ros88 Ross S. and Morrison I.D. "Colloidal Systems and Interfaces." New York: Wiley (1988).
- Rya96 Ryan J.N. and Elimelech M. Colloids Surf. A: 107 1-56 (1996).
- Sca92 Scales P.J. Grieser F. Healy T.W. White L.R. and Chan D.Y.C. Langmuir 8 (3) 965-974 (1992).
- Sch94 Schamhart D.H. de Boer E.C. and Kurth K.H. World J. Urol. 12 (1) 27-37 (1994).
- Sch91 Schwertmann U. and Cornell R.M. "Iron Oxides in the Laboratory: Preparation and Characterization." Weinheim, Germany: VCH Verlag Chap. 5 (1991).
- She85 Sherman P.M. Houston W.L. and Boedeker E.C. Infect. Immun. 49 (3) 797-804 (1985).
- Sim88 Simonsson T. Glantz P.O. Edwardsson S. and Olsson J. Acta Odontol Scand. 46 (3) 177-180 (1988).
- Sim91a Simonson T. Perahia D. Bricogne G. J. Mol. Biol. 218 (4) 859-886 (1991).
- Sim91b Simonson T. Perahia D. Brunger A.T. Biophys. J. 59 (3) 670-690 (1991).
- Smi93 Smith J.L. J. Food Protection 56 (5) 451 (1993).
- Som98 Somasundaran P. Yu X. Krishnakumar S. Colloids and Surfaces A: 133 (1-2) 125-133 (1998).
- Son94 Song L. Johnson P.R. and Elimelech M. Environ. Sci. Technol. 28 1164-1171 (1994).
- Spi73 Spielman L.A. Friedlander S.K. J. Colloid Interface Sci. 46 (1) 22-31 (1973).

- Ste89 Steadman R. Topley N. Knowlden J.M. Mackenzie R.K. Williams J.D. Biochim. Biophys. Acta **1013** (1) 21-27 (1989).
- Ste94 Stenkamp V.S. and Benjamin M.M. Amer. Wat. Wor. Ass. **86** (Aug.) 37-50 (1994).
- Ste85 Stenstrom T.A. and Kjelleberg S. Arch. Microbiol. **143** (1) 6-10 (1985).
- Ste89 Stenstrom T.A. Appl. Environ. Microbiol. **55** 142-147 (1989).
- Suh95 Suhara T. Fukui H. and Yamaguchi M. Colloids Surf. A **95** (1) 29-37 (1995).
- Sur97 Suresh L. and Walz J.Y. J. Colloid Interface Sci. **196** (2) 177-190 (1997).
- Tat87 Tatulian S.A. Biochim. Biophys. Acta **901** (1) 161-165 (1987).
- Tem81 Temple P.A. Applied Optics **20** 2656 (1981).
- Tum97 Tuminello P.S. Applied Optics **36** (13) 2818(7) (1997).
- van80 van der Put A.G. "Electrokinetic Investigations on the System Polystyrene/Aqueous Electrolyte Solution." Ph.D. Thesis Wageningen, The Netherlands: Agricultural University of Wageningen (1980).
- van96 van der Waal A. "Electrochemical Characterization of the Bacterial Cell Surface." Ph.D. Thesis Wageningen, The Netherlands: Wageningen Agricultural University (1996).
- van97a van der Waal A. Minor M. Norde W. Zehnder A.J.B. and Lyklema J. Langmuir **13** 165-171 (1997).
- van97b van der Waal A. Minor M. Norde W. Zehnder A.J.B. and Lyklema J. J. Colloid Interface Sci. **186** 71-79 (1997).
- Van90 Vanhaecke E. Remon J.P. Moors M. Raes F. De Rudder D. and Van Peteghem A. Appl. Environ. Microbiol. **56** (3) 788-795 (1990).
- vanI84 van Iterson W. ed. "Outer Structures of Bacteria -Benchmark Papers in Microbiology." New York: van Nostrand Reinhold 135 (1984).
- vanK95 van Keulen H. and Smit J.A.M. J. Colloid and Interface Sci. **170** (1) 134-145 (1995).
- vanL87a van Loosdrecht M.C.M. Lyklema J. Norde W. Schraa G. Zehnder A.J.B. Appl. Environ. Microbiol. **50** (8) 1898-1901 (1987).

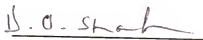
- vanL87b van Loosdrecht M.C.M. Lyklema J. Norde W. Schraa G. Zehnder A. J. B. Appl. Environ. Microbiol. 53 (8) 1893-1897 (1987).
- vanL90 van Loosdrecht M.C.M. Norde W. and Zehnder A.J. J. Biomater Appl. 5 (2) 91-106 (1990).
- VanW80 Van Wagenen R.A. and Andrade J.D. J. Colloid and Interface Sci. 76 305 (1980).
- Ver48 Verwey E. and Overbeek J. Th. G. "Theory of the Stability of Lyophobic Colloids." Amsterdam: Elsevier Publishing (1948).
- Vit91 Vitaya V.B. and Toda K. Biotechnol. Prog. 7 (5) 427-433 (1991).
- Wal98 Walz J.Y. Advances in Colloid and Interface Science 74 (1-3) 119-168 (1998).
- War94 Warwicker J. J. Mol. Biol. 236 (3) 887-903 (1994).
- Wat92 Watanabe K. Yamaji Y. and Umemoto T. Oral Microbiol. Immunol. 7 (6) 357-363 (1992).

## BIOGRAPHICAL SKETCH

Stephen Edward Truesdail was born in Willoughby, Ohio, on June 17, 1971. He received his Bachelor of Science degree in chemical engineering from Purdue University in May of 1993. In July of that year he married Viktoria Lynne Vazach. He entered the doctoral research program in the department of chemical engineering at the University of Florida in 1994 and received his Ph.D. in May 1999.



I certify that I have read this study and that in my opinion it conforms to acceptable standards of scholarly presentation and is fully adequate, in scope and quality, as a dissertation for the degree of Doctor of Philosophy.



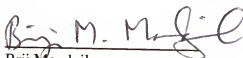
Dinesh O. Shah, Chair  
Professor of Chemical Engineering

I certify that I have read this study and that in my opinion it conforms to acceptable standards of scholarly presentation and is fully adequate, in scope and quality, as a dissertation for the degree of Doctor of Philosophy.



Richard B. Dickinson, Co-Chair  
Assistant Professor of Chemical  
Engineering

I certify that I have read this study and that in my opinion it conforms to acceptable standards of scholarly presentation and is fully adequate, in scope and quality, as a dissertation for the degree of Doctor of Philosophy.



Brij Moudgil  
Professor of Materials Science and  
Engineering

I certify that I have read this study and that in my opinion it conforms to acceptable standards of scholarly presentation and is fully adequate, in scope and quality, as a dissertation for the degree of Doctor of Philosophy.



Raj Rajagopalan  
Professor of Chemical Engineering

I certify that I have read this study and that in my opinion it conforms to acceptable standards of scholarly presentation and is fully adequate, in scope and quality, as a dissertation for the degree of Doctor of Philosophy.



---

Samuel Farrah  
Professor of Microbiology and Cell  
Science

This dissertation was submitted to the Graduate Faculty of the College of Engineering and to the Graduate School and was accepted as partial fulfillment of the requirements for the degree of Doctor of Philosophy.

May 1999



---

Winfred M. Phillips  
Dean, College of Engineering

---

M. J. Ohanian

Dean, Graduate School